Controls on the stability and composition of amphibole in the Earth's mantle

Controls on the stability and composition of amphibole in the Earth's mantle

Ben E. Mandler*[1] & Timothy L. Grove[1]

[1]Department of Earth, Atmospheric and Planetary Sciences, Massachusetts Institute of Technology, 77 Massachusetts Avenue, Cambridge MA 02139.

*Corresponding author: bmandler@mit.edu, 617-774-7227

Keywords: experimental petrology; amphibole; peridotite; mantle; metasomatism; thermobarometry

Abstract

Presented here is a suite of new experiments aimed at quantifying the effects of pressure, temperature, bulk composition and H_2O content on the stability and composition of amphibole in the Earth's mantle. Experiments have been performed from 2-4 GPa and 950–1100 °C on fertile and depleted mantle compositions. H_2O contents of most experiments are 0.65 wt.%. In the fertile mantle composition, pargasitic amphibole is stable up to ~3.8 GPa at 1000 °C, approximately 0.5 GPa higher than any previous study. The upper stability limit of amphibole in depleted mantle is 0.7 GPa and 40 °C lower than in fertile mantle. The addition of 3 wt.% H_2O to fertile mantle destabilizes amphibole by 0.5 GPa and 40 °C relative to the 0.65 wt.% H_2O experiments. Compared to existing experiments on amphibole stability, these experiments

indicate that pargasitic amphibole may be stable in mantle lithosphere to almost 4 GPa (0.5 GPa higher (15 km deeper) than previously thought). The extremely strong destabilizing effect of H_2O suggests that deeper portions of the strongly fluid-fluxed mantle wedge may be amphibole-free even at low temperatures near the slab-wedge interface. The molar alkali content of amphibole is shown to be a linear function ($R^2 = 0.98$) of pressure and temperature and is relatively insensitive to bulk compositional differences between fertile and depleted mantle. This relationship is used to produce an empirical thermobarometer for pargasite-bearing spinel- and garnet- lherzolites. Comparison to existing experimental data shows that this thermobarometer has predictive ability over the pressure range of 1 to 4 GPa. Comparisons with pressure-temperature estimates of garnet+amphibole peridotites further corroborate the applicability of this thermobarometer for natural samples. Pressure estimates are presented for four examples of metasomatized spinel peridotites otherwise lacking pressure information, and future avenues for refinement of the thermobarometer are discussed.

Introduction

The Earth's uppermost mantle is pervasively metasomatized, as illustrated by dozens of exhumed peridotite massifs and thousands of mantle xenoliths. Metasomatic agents come in many flavors, from H_2O-rich fluids to silicate melts, but almost all metasomatized mantle samples are enriched in H_2O and fluid-mobile elements. The most abundant of these elements are the alkalis Na and K, so the most common new minerals formed during mantle metasomatism are alkali-bearing hydrous silicates (amphiboles and micas). Because these minerals both store H_2O when they form, and release it when they break down, they exert a

strong control on the geodynamic and geochemical behavior of the mantle lithosphere. Specifically, the pressure-temperature (P-T) stability fields of amphiboles and micas play critical roles in: (i) the extent to which H_2O is released into the overlying mantle wedge at subduction zones or transported to the deep mantle; (ii) the water storage capacity of the uppermost mantle; and (iii) the generation of alkaline, hydrous magmas in intraplate settings due to hydrous melting triggered by the high-P-T breakdown of these phases during delamination or thermal perturbation. Furthermore, the strong P-T-dependence of the composition of amphibole (e.g. Niida and Green 1999) suggests that a calibration of these effects may yield a viable thermobarometer for amphibole-bearing mantle samples.

In this study we present new experiments that rigorously assess the effects of pressure, temperature, bulk composition and H_2O content on the stability and composition of amphibole in the uppermost mantle. The need for such a study has become apparent over the past several decades, during which many investigations of amphibole stability have been published, producing a wide range of pressure- and temperature stability limits (Figure 1). Some of the apparent problems have been identified but not quantified, and uncalibrated interlaboratory differences make a collated analysis difficult. The two most significant problems, and those we focus on in this paper, are the effects of bulk composition and H_2O content on amphibole stability and composition. By isolating each variable over a range of pressures and temperatures, we can identify the effects of all four variables (P, T, X, H_2O) and provide quantitative information on some of the factors that influence the behavior of this notoriously complex mineral group in mantle lithologies.

Previous work

Early work showed that the stability field of amphibole was not only pressure-invariant at high temperatures but also nearly temperature-invariant at high pressures (Gilbert 1969; Kushiro 1970; Green 1973; Mysen and Boettcher 1975). Both the pressure and temperature stability limits were shown to be dependent on several important factors:

Bulk composition. Mysen and Boettcher (1975) clearly showed that amphibole stability was dependent on bulk composition. Subsequent work by Wallace and Green (1991) showed that more alkali-rich, fertile mantle compositions stabilize amphibole to higher P and T than more depleted compositions. Since then, it has been repeatedly shown that compositions rich in alkalis tend to stabilize amphibole to the highest pressures and temperatures (e.g. Niida and Green 1999; Fumagalli et al. 2009), but this effect has yet to be quantified.

H_2O content. It has long been recognized that the upper stability limit of hydrous phases depends on the H_2O content of the system. Yoder and Kushiro (1969) suggested, based on a study of phlogopite, that hydrous phases are most stable when the bulk H_2O content of the system is equal to that of the hydrous phase in question (4 wt.% for phlogopite, 2 wt.% for amphibole). However, the experimental literature suggests that even small amounts of excess H_2O can leach amphibole-stabilizing alkalis into a fluid phase and thus induce amphibole breakdown at lower-P-T conditions. An amphibole-bearing peridotite containing no other hydrous phases will have a bulk H_2O content of only 0.2-0.3 wt.%, and Green et al. (2014) have recently shown that bulk H_2O contents as low as 1 wt.% are sufficient to decrease amphibole stability. This helps to explain the relatively small amphibole stability fields found by Kushiro (1970; >5.8 wt.% H_2O), Green (1973; 6 wt.% H_2O in water-saturated experiments), Millhollen et

al. (1974; 5.7 wt.% H_2O), Mysen and Boettcher (1975; >8 wt.% H_2O), and Grove et al. (2006; 14.5 wt.% H_2O). This effect is the single largest control on amphibole stability in experiments (Figure 1), yet it remains very poorly constrained.

Oxygen fugacity. Early studies on simple Fe^{3+}-rich amphibole systems showed that relatively huge fO_2 variations (5 log units) could change the stability field of Fe^{3+}-rich amphiboles by ~100 °C (Ernst 1962; Gilbert 1966). The implications for mantle samples, however, are only minor because (1) amphiboles in equilibrium with peridotite are very poor in iron (Mg# ~ 90), and (2) the total range in oxygen fugacity for all mantle samples within the relevant pressure range is ~4 log units, from reduced Archean cratons to oxidized subduction zones (Frost and McCammon 2008). We therefore do not consider the effects of fO_2 in this study.

There has been significant recent interest in the geodynamic roles played by amphibole and other hydrous minerals (e.g. Green et al. 2010; van Keken et al. 2011; Wada et al. 2012; Walowski et al. 2015). Of particular interest are water storage and release during subduction, and the depth to which amphibole is stable in the oceanic and continental lithosphere. These problems require a rigorous and quantitative understanding of the controls on the stability of amphibole in the upper mantle, which we aim to provide here. Having done this, we will evaluate the potential for the compositional variability of mantle amphiboles to be harnessed as a thermobarometer.

Experimental Methods

111 *Starting compositions*

112 To accurately quantify the behavior of amphibole in the Earth's uppermost mantle, it is
113 important to use realistic mantle compositions that span a typical range of mantle compositions.
114 To do this, we inspected the peridotite xenolith compositions in the GEOROC database
115 (http://georoc.mpch-mainz.gwdg.de/georoc/) and chose a fertile and a depleted composition
116 (Table 1). The fertile composition (FNa) was determined by taking the MgO content of the
117 primitive upper mantle estimate of Hart and Zindler (1986) – 37.8 wt.% – and adjusting the other
118 elements to produce a composition representative of peridotite xenoliths with that MgO content
119 (Figure 2). These adjustments were all small and were conducted to make the composition as
120 representative as possible of common xenolith compositions. Compositions were checked
121 against real xenolith compositions in terms of all elements incorporated into the starting mix to
122 ensure a realistic composition. The depleted composition (DNa) was also chosen to be
123 representative of mantle xenoliths, and corresponds approximately to the residue after 20% melt
124 extraction from a fertile peridotite as calculated by Walter (1999).

125 Both fertile and depleted compositions were modified by adding 1 wt.% of a metasomatic
126 component made of 65% H_2O, 30% Na_2O and 5% K_2O (values in wt.%). This metasomatic
127 component was based on compositional estimates for slab-derived fluids/melts at subduction
128 zones, which are H_2O- and alkali-rich (Stolper and Newman 1994; Keppler 1996; Scambelluri
129 and Philippot 2001; Grove et al. 2002). The slab-derived component may also contain other
130 components (e.g. Al, Si, Ca), particularly if it is a melt, but the major elements in peridotite will
131 be negligibly affected by 1 wt.% addition of the metasomatic component. A third bulk

composition (FNa3) was used to investigate the effect of H_2O on amphibole stability; FNa3 consists of composition FNa with additional H_2O added to give 3 wt.% H_2O in the bulk.

The resulting starting compositions (Table 1) are representative of metasomatized mantle samples and sample both fertile and depleted compositions. Although some prior experimental studies have investigated depleted peridotites (Mengel and Green 1989; Wallace and Green 1991; Fumagalli et al. 2009), the experiments were conducted on depleted compositions that had 30-60% olivine subtracted from their bulk. Olivine subtraction introduces additional uncertainty due to assumptions made about the composition of olivine to remove, and results in bulk compositions that have some depleted signatures (e.g. high Cr/Al and low Fe/Mg ratios) but some enriched ones (e.g. high Na/Si and Al/Mg ratios). To avoid the uncertainty associated with olivine subtraction, we have not performed this step on our depleted composition. This study is therefore the first to present detailed information on amphibole stability and composition in a depleted peridotite that has not been modified outside the range of natural depleted peridotite compositions (Figure 2).

Starting materials

All starting materials were synthesized from high-purity oxides (SiO_2, TiO_2, Al_2O_3, Cr_2O_3, Fe_2O_3, MnO, MgO, NiO), carbonates (Na_2CO_3, K_2CO_3), metallic Fe, and synthetic silicates ($CaSiO_3$) and hydroxides ($Mg(OH)_2$). All materials except for the Fe- and H_2O sources were dried in furnaces, then weighed out and ground together under ethanol for 3 hours using an agate pestle and mortar. These were decarbonated at 850 °C for 1-2 days before FeO was added by mixing Fe_2O_3 and metallic Fe together in appropriate molar proportions. The Fe-bearing mix was

then ground under ethanol for another hour, dried and conditioned for 3 days at 1050 °C and an fO_2 of 0.5 log units above the quartz-fayalite-magnetite buffer. H_2O was added to mixes FNa and DNa using synthetic brucite ($Mg(OH)_2$) to precisely control the H_2O content at 0.65 wt.%. A final grinding under ethanol for one hour evenly distributed this H_2O source in the starting material. The additional H_2O for mix FNa3 was added by microsyringe to each capsule immediately prior to welding. Weighing of the capsule before and after welding confirmed that H_2O loss during the welding process was negligible (<0.00001 g).

Experimental procedures

All experiments were performed using Au capsules. These were fabricated from Au tubing with an inner diameter of 0.13" and a wall thickness of 0.01". Tubing segments ⅜" long were cut from tubing stock and triple-crimped on one end. This end was then welded using a PUK U3 TIG welder and flattened to produce a uniformly thick and flat capsule top. The capsule was then filled with ~0.06 g of starting material, which was packed down into the capsule. The unfilled portion of the capsule was cleaned to ensure a good weld. For FNa3 runs, additional H_2O was added at this point to yield 3 wt.% in the bulk, using a microsyringe and a scale to ensure precise control over the amount of H_2O added. The bottom of the capsule was then triple-crimped and welded shut. The sealed capsule was flattened in a die to produce a final capsule length of 0.15", then placed in an alumina ring and centered in a graphite furnace using MgO spacers.

Experiments were conducted at the MIT experimental petrology laboratory with a 0.5" solid medium piston-cylinder apparatus (Boyd & England, 1960) using the hot-piston-in technique (Johannes et al., 1971). The pressure medium was $BaCO_3$, for which no pressure

correction was deemed necessary based on pressure calibration of this apparatus using the reaction: anorthite + gehlenite + corundum = Ca-Tschermak's pyroxene, and the spinel to garnet transition in the CMAS peridotite analog system (1500°C, 2.5 GPa) (Longhi 2005). Pressures are considered accurate to ±50 MPa. Temperatures were measured and controlled with type-D ($W_{97}Re_3$-$W_{75}Re_{25}$) thermocouples linked to a Eurotherm 831 controller. No EMF correction was applied for pressure effects on the thermocouple. Reported temperatures are considered accurate to ±10 °C. The thermal structure of the run assembly in this apparatus was previously determined to have a 20 °C temperature gradient between the thermocouple junction and the hotspot of the furnace (for which a correction was applied to the run temperature), and a temperature gradient across the capsule of ~10 °C (Medard et al., 2008). Each experiment was initiated by manually raising the pressure to 1 GPa at room temperature. The temperature was then increased to 865 °C at a rate of 100 °C/min. As the $BaCO_3$ cell compressed, the pressure was manually raised to keep it at 1 GPa. The run was held at 865 °C for 6 minutes, during which time the pressure was raised to the final run pressure. The temperature was then ramped to the final run temperature at a rate of 50 °C/min, with further manual pumping of the pressure system to maintain the pressure at the final run pressure. The pressure typically stabilized after ~30 minutes. Run durations at these conditions were 4-7 days (Table 2). The experiments were terminated by turning off the power to the furnace. The capsule was extracted and a small hole was drilled to check for excess H_2O, then the capsule was cut into 4 thin slices using a diamond wire saw. These slices were vacuum-impregnated with epoxy, mounted in an epoxy disc, polished with alumina, and carbon-coated to prepare them for electron microprobe analysis.

198 *Analytical methods*

199 All samples were analyzed using the JEOL JXA-8200 Superprobe at MIT. Backscattered
200 electron imaging, energy-dispersive spectrometry and chemical mapping were used to inspect the
201 mineralogy and appearance of the run. Phase compositions were obtained by wavelength-
202 dispersive spectrometry, using a focused electron beam (spot size ~1 μm) with a 15 kV
203 accelerating voltage and a 10 nA beam current. Count times for Na were varied to assess the
204 significance of undercounting due to Na migration. A count time of 10 s was ultimately used for
205 Na, which provided sufficiently high counts for consistent, suitably precise analyses without any
206 measurable Na loss. The rest of the elements were all counted for 40 s (no K migration problems
207 were observed). Data were reduced using the CITZAF correction package (Armstrong, 1995),
208 then manually inspected for data outliers produced by the beam partially hitting minerals other
209 than the one intended for analysis. This was a particularly acute problem for the highly poikilitic
210 garnets, which is reflected by the small number of points analyzed for garnet in some of the
211 experiments (Supplementary Table 4).

212

213 **Results**

214 Experimental conditions and phase assemblages are given in Table 2. Chemical analyses of
215 experimentally produced amphiboles are given in Table 3. Chemical analyses of all other phases
216 are given in the supplementary information.

217

218 *Equilibrium, quench alteration, and oxygen fugacity in experiments*

Experimental durations exceeding a few days were enough to achieve equilibrium. This was confirmed by several observations: (i) internal chemical homogeneity of solid phases; (ii) constancy of solid phase compositions and equilibrium crystal textures across the entire charge; and (iii) systematic and predictable variability of solid phase compositions between experiments at different pressures and temperatures. In the 1100 °C experiments, quench crystals were common but easily identified by their acicular habit (Figure 3d) and melt-like chemistry (e.g. quench amphiboles with Mg# = 77, cf. equilibrium amphiboles with Mg# ~ 90). Only equilibrium phase compositions are reported here.

Four of the experiments had spinel, orthopyroxene and olivine present, making oxygen fugacity estimates possible using the oxybarometer of Ballhaus et al. (1991). Two of these experiments (D288 and D293) gave an oxygen fugacity of QFM + 0.4, while the other two (D292 and D304) indicated more reducing conditions of QFM –1 to –2. This range is broadly similar to that estimated by Grove et al. (2006) for very similar experiments (QFM –1 to +2). We therefore infer that the oxygen fugacity of this suite of experiments was within this range. This indicates a bulk $Fe^{3+}/\Sigma Fe$ of ≤ 0.15 (Kress and Carmichael 1991). The presence of a small fraction of Fe^{3+} is important for understanding some of the substitution reactions controlling the phase chemistry in these experiments – see below.

Phase relations

Figure 3 shows the typical appearance of experimental charges at different conditions. Figure 4 shows the pressure-temperature stability fields for the minerals observed in the three experimental series. Melt was present in all experiments, as determined by the presence of glass

241 wisps connecting minerals in all runs, and quench crystals in 1100 °C runs. Melt pockets were
242 plucked out by the polishing process but were identified in backscattered electron images as open
243 spaces with few crystals; these areas were routinely observed in the hottest portion of the charge,
244 especially in 1050 and 1100 °C runs.

245 A free fluid phase was observed when capsules were drilled open after each experiment,
246 but this does not necessarily mean that a free fluid phase was present at the temperature and
247 pressure of the experiment. In compositions FNa and DNa (cf. FNa3), and at higher
248 temperatures, it is likely that sufficient melt was present to incorporate all of the H_2O. For a bulk
249 H_2O content of 0.65 wt.% and a high-pressure melt H_2O solubility of 20-30% (Hodges 1972;
250 Pirard and Hermann 2015), only 2-3% melt is required to incorporate all of the H_2O even if no
251 amphibole is present. The presence of amphibole (2 wt.% H_2O) reduces the melt fraction
252 required to incorporate all H_2O without the need for a free fluid phase. It is therefore likely that
253 in the FNa and DNa experiments the fluid observed during the drilling of capsules after each run
254 was dissolved in the melt at run conditions but exsolved upon quenching, producing
255 interconnected fluid and shards or wisps of glassed melt. In FNa3 experiments, there was almost
256 certainly a free fluid phase at run conditions due to the much higher bulk H_2O content.

257 Olivine is observed in all experiments. Crystals are hypidiomorphic to xenomorphic,
258 equant, and range in size from ~5 μm in the 950 °C experiment up to 30 μm in 1100 °C
259 experiments. In runs of all pressures, some crystals contain tiny (<< 1 μm) Al-Cr-rich inclusions,
260 which are remnants of spinels trapped by olivine growth during the pressure-temperature
261 ramping at the start of each experiment.

Orthopyroxene is observed in all experiments. Crystals are hypidiomorphic to idiomorphic, stubby to elongate, and range from 10 μm long in the 950 °C experiment up to 70 μm long in 1100 °C experiments. They commonly contain small (~1-3 μm) inclusions of clinopyroxene.

Clinopyroxene is observed in all experiments. However, in the highest-temperature (1100 °C) experiments, clinopyroxene is only observed in the coolest portions of the charge, indicating that these experiments were very close to the upper temperature limit for clinopyroxene. Crystals are hypidiomorphic to idiomorphic, equant in shape, and range from ~5 μm in the 950 °C experiment up to ~15 μm in the 1100 °C experiments.

Garnet is observed in all of the highest-pressure experiments. For composition FNa, garnet is observed at all pressures greater than 2 GPa. However, in composition DNa, garnet is only observed at pressures greater than 2.5 GPa. This is due to the much higher Cr/Al ratio of composition DNa (Table 1), which stabilizes spinel over garnet to higher pressures (O'Neill 1981; Carroll Webb and Wood 1986; Klemme 2004; Ziberna et al. 2013). Crystals are large (up to 100s of μm), hypidiomorphic to perfectly idiomorphic, and extremely poikilitic, containing inclusions of all other mineral phases. The strong favoring of growth over nucleation and the very low availability of inclusion-free areas for analysis are likely responsible for the greater compositional scatter observed in garnet analyses compared to other solid phases (Supplementary Table 4).

Spinel is observed in very few experiments. This is because at low pressures amphibole provides a sufficiently large sink for Al that another aluminous phase is not required (at high pressure, the lower abundance and lower Al content of amphibole is accompanied by garnet

stability). Amphibole and spinel only coexist in one experiment (Figure 4). Spinel is therefore observed only in the highest-temperature DNa and FNa3 experiments, in which amphibole is significantly destabilized. This is consistent with the observations of Fumagalli et al. (2009), who performed experiments up to only 1000 °C and so never observed any spinel. In experiments that do have spinel, crystals are rare (<1% of the charge), small (1-3 μm), hypidiomorphic and equant.

Amphibole is observed in most experiments. As shown by Figure 4, its upper pressure stability limit approaches temperature invariance, while its upper temperature stability limit approaches pressure invariance. Its upper pressure limit is largely controlled by the progressive up-pressure stabilization of garnet and the jadeitic clinopyroxene component, which sequester many of the elements necessary for amphibole stability (notably Al, Cr, and Na). Because amphibole is a hydrous mineral, its upper temperature limit is controlled by the dehydration reactions that release H_2O into the melt phase. Amphibole crystals are stubby to elongate and hypidiomorphic, ranging from ~5 μm long in the 950 °C experiment, up to 20 μm long in some 1050 °C experiments.

Phase compositions

All phases show systematic compositional changes as a function of pressure and temperature, as well as compositional differences between the two bulk compositions. In general, phases in the DNa experiments have higher Mg# and Cr_2O_3, and lower TiO_2, than in the FNa experiments. Major elements that are much less abundant in the DNa bulk composition (Ca, Al) are only mildly depleted in the minerals; the bulk depletion of these elements is instead recorded by the

lower abundance of Ca- and Al-bearing minerals (clinopyroxene and garnet). Most of the same pressure-temperature compositional trends are observed in both the FNa and DNa experiments. The few that are not resolved in the DNa experiments (MnO and Mg# in opx, cpx, and amphibole) are largely due to the small number of experiments on the DNa composition. The chemical systematics described below are based on the FNa experiments, for which the coverage of pressure-temperature space is much more thorough. Some of the most significant pressure effects are shown in Figure 5 for the 1000 °C FNa runs.

Olivine and orthopyroxene compositions become progressively Mn- and Fe-poor, and Mg-rich, with increasing pressure and temperature. Orthopyroxene additionally becomes progressively Ca-, Al- and Cr-poor, and Si-, Na- and (Mg+Fe)-rich with increasing pressure. This is due to two main substitution reactions: (1) the high-pressure destabilization of the Tschermak-type component and other associated trivalent components: $2\ (Al,Cr,Fe)^{3+} \Leftrightarrow (Mg,Fe)^{2+} + Si^{4+}$; and (2) The slightly decreased solubility of Ca in the orthopyroxene structure at high pressure: $Ca^{2+} \Leftrightarrow (Mg,Fe)^{2+}$. The small Na increase in orthopyroxene with increasing pressure is due to the stabilization of a minor Na-bearing component at high pressure. The effects of temperature on orthopyroxene composition are largely the inverse of the pressure effects: higher temperatures stabilize the Tschermak-type and other trivalent components, and increase the solubility of Ca in the orthopyroxene structure (the latter representing the up-temperature closing of the orthopyroxene–clinopyroxene two-phase region). As a result, higher temperatures make orthopyroxene more Ca-, Al-, and Cr-rich, and more (Mg+Fe)-poor. The effect of temperature on Si is not well resolved because the expected decrease in Si concentration is of the same order as the analytical uncertainty.

Clinopyroxene shows more complex behavior than orthopyroxene, with three important substitution reactions producing several effects. (1) The dominant substitution reaction is the stabilization of a jadeite (or other Na-bearing) component with increasing pressure: Ca^{2+} + $(Mg,Fe)^{2+} \Leftrightarrow Na^{+} + (Al,Cr,Fe)^{3+}$. With increasing pressure, this produces a decrease in Ca and Mg, and an increase in Na and Cr (Figure 5). (2) The high-pressure destabilization of the Tschermak-type component (as in orthopyroxene) offsets the up-pressure increase in Al from the Na-bearing component, and complicates the behavior of Fe, which, due to its multiple valence states, is involved on both sides of both reactions. These two competing substitutions explain why Al only increases slightly with pressure while Na increases a lot, and why the Mg# of clinopyroxene is not strongly correlated with pressure (Figure 5). As in orthopyroxene, the Tschermak-type component is stabilized at higher temperatures, producing higher Al and lower (Mg+Fe) concentrations. (3) The third substitution reaction is the substitution $Ca^{2+} \Leftrightarrow (Mg,Fe)^{2+}$, which produces an up-temperature decrease in clinopyroxene Ca content and offsets the temperature effects of the substitution of Ca for Mg and Fe related to the enhanced Ca-Tschermak solubility in clinopyroxene.

Amphibole shows highly systematic compositional variability as a function of pressure (Figure 5) and temperature. Amphiboles are broadly pargasitic ($NaCa_2(Mg_4Al)Si_6Al_2O_{22}(OH)_2$), with some K in the A site and Fe in the M1, M2, and M3 sites. With increasing pressure, amphiboles show a significant substitution towards richterite ($Ca^{2+} + (Al,Fe,Cr)^{3+} + 2\ Al^{3+} \Leftrightarrow Na^{+} + Mg^{2+} + 2\ Si^{4+}$), with minor substitutions towards magnesiokatophorite ($Ca^{2+} + Al^{3+} \Leftrightarrow Na^{+} + Si^{4+}$) and possibly edenite ($(Al,Fe,Cr)^{3+} + Al^{3+} \Leftrightarrow Mg^{2+} + Si^{4+}$). Mg# increases with temperature and pressure, and high temperatures lead to lower Si and Ca, and higher Na. The up-

temperature increase in Na appears to be due to a coupled substitution with both Al and Fe^{3+}. K contents increase substantially with both pressure and temperature, akin to the behavior of Na. Notably, the Na_2O and K_2O contents of amphiboles in DNa, FNa and FNa3 experiments are almost indistinguishable, despite varying alkali and H_2O contents in the bulk (see discussion).

Garnet compositions become increasingly pyrope-rich at higher temperatures and grossular-poor at higher pressures. Slightly higher Fe and lower Al contents at high pressures suggest a minor $Al^{3+} \Leftrightarrow Fe^{3+}$ substitution. There is no resolvable change in Mg# with pressure, as both MgO and FeO are mildly increased at high pressures. Garnets in the DNa experiments have ~0.7 mol% lower Al_2O_3 and correspondingly higher Cr_2O_3 than the equivalent experiments on the FNa composition.

Spinel is only present in one FNa3 and three DNa experiments, and shows no systematic compositional change with pressure, temperature or bulk composition. The Mg# ranges from 62 to 68; the Cr# (100Cr/(Cr+Al)) ranges from 49 to 59.

Discussion

Compositional controls on the stability of amphibole in the mantle

A number of compositional variables control the stability and composition of amphibole in the Earth's mantle. We will explore the most important of these and, where possible, quantify their influence on amphibole stability.

Experiments by Green and coworkers showed that higher bulk abundances of elements compatible in amphibole but less so in other mantle minerals (alkalis and perhaps Ti) will

372 increase amphibole's pressure-temperature stability (Wallace and Green 1991). Fertile mantle
373 compositions should therefore stabilize amphibole to higher pressures and temperatures than
374 depleted ones. This idea is reinforced by our experiments: the upper stability limit of amphibole
375 in the depleted composition is 0.7 GPa and 40 °C lower than in the fertile composition (Figure
376 6).

377 However, the idea of fertile and depleted peridotite is complex and depends on the nature
378 of the metasomatizing agent responsible for refertilization. Depletion and refertilization of
379 peridotites by the removal or addition of basaltic melts have somewhat predictable effects, but
380 the addition of slab-derived fluids and slab melts (of sediments and/or basalts) at subduction
381 zones produces a much wider range of compositions. The resulting effects on amphibole stability
382 will depend on the nature of the added material and can vary in many ways.

383 The recent work of Pirard and Hermann (2015) provides a compositionally extreme but
384 plausible example of this variability. They have shown that an ultradepleted peridotite/dunite that
385 is refertilized by a Ca-poor, alkali-rich sediment melt will stabilize amphibole to higher pressures
386 (> 4.5 GPa) than typical fertile peridotite (< 4 GPa, this study). This is probably due to the
387 absence of clinopyroxene in low-Ca bulk compositions: in Ca-richer peridotites, the up-pressure
388 stabilization of the jadeitic clinopyroxene component ($NaAlSi_2O_6$) limits the stability of Na-
389 bearing amphibole. In the absence of clinopyroxene, there is no major Na-bearing phase to
390 replace amphibole at higher pressures, so a very Na+K-rich, Ca-poor amphibole
391 (magnesiokatophorite) remains stable at high pressure, as long as there are sufficiently high
392 alkali contents in the bulk composition.

393 This is just one facet of a much larger problem. Work by Konzett and Ulmer (1999) and
394 Fumagalli et al. (2009) on the same bulk composition suggests that in systems sufficiently K-rich
395 to stabilize phlogopite there are actually two stability fields for amphibole (Figure 7): a more
396 sodic amphibole at lower pressure, and a more potassic amphibole at much higher pressure
397 resulting from the high-pressure breakdown of phlogopite. In systems too K-poor to stabilize
398 phlogopite (K_2O < ~0.1 wt.%), the K_2O released upon amphibole breakdown goes into the melt
399 at high temperatures, and clinopyroxene (0.1-0.4 wt.% K_2O at 6-8 GPa; Konzett and Ulmer
400 1999) and trace grain-boundary phases at lower temperatures.
401 A third issue is the stability of kaersutitic (Ti-rich) and Ti-pargasitic amphiboles, formed
402 by low-pressure, high-temperature metasomatism of peridotites by hydrous, alkaline, Ti-rich
403 basaltic melts. Furthermore, although Ti-rich (several percent TiO_2) amphiboles are generally
404 restricted to the spinel stability field, a Ti-component (0.5-0.7 wt.%) in amphibole remains up to
405 very high pressures, (e.g. amphiboles in PKP and MARID xenoliths from kimberlites; Konzett
406 and Ulmer 1999). The effect of Ti on amphibole stability has yet to be resolved, but the overall
407 effect seems to be a stabilizing one.
408 The effects of most of these variables on amphibole stability have yet to be quantified.
409 However, we can make several statements about the effects of bulk composition on the stability
410 of amphibole (see Figure 8 for a schematic summary), based on prior work and new insights
411 provided by this study:
412 (1) High alkali contents stabilize amphibole to higher pressures and temperatures
413 (Wallace and Green 1991; this study)

(2) High bulk Na/Ca ratios ($Na_2O/CaO > \sim0.5$?) stabilize a highly sodic amphibole to higher pressures at the expense of clinopyroxene (Pirard and Hermann 2015; this study)

(3) While the highly sodic amphiboles produced by high bulk Na/Ca ratios (i.e. low Ca) are very pressure-stable, these high-Na/Ca amphiboles have lower temperature stability limits than pargasitic amphiboles. In simple systems the practically Ca-free sodic amphibole glaucophane is only stable up to 800 °C (Tropper et al. 2000); magnesiokatophorite ($Na_2O/CaO \sim 2$) is stable in ultra-Ca-depleted peridotites to ~1000 °C (Pirard and Hermann 2015); and pargasite ($Na_2O/CaO < 0.5$) is stable in fertile and depleted peridotites to at least 1100 °C (this study). Higher bulk Ca contents stabilize amphibole to higher temperatures, although there does not seem to be any benefit to increasing bulk Ca content beyond that necessary to stabilize pargasite.

(4) Ti (and possibly Cr) stabilizes amphibole, but has unclear effects on its upper stability limit (Wallace and Green 1991; this study). The range of natural variability in the abundance of other elements (Al, Si, Fe and Mg) appears not to have significant effects on amphibole stability.

(5) Free H_2O destabilizes amphibole by leaching amphibole-stabilizing elements into a fluid phase. See section "Effects of H_2O on the stability and composition of amphibole", below, for further details.

The effects of these variables have yet to be fully quantified, but the results of our experimental study allow the development of a framework for interpretating natural samples, and suggest avenues for future experimental investigations into amphibole stability.

435 *Controls on the composition of amphibole in the mantle: developing a thermobarometer for*
436 *metasomatized peridotites*
437 The experiments presented here show that amphibole composition follows an extremely
438 systematic and predictable dependence on pressure and temperature. The variations in the molar
439 abundance of $Na_2O + K_2O$ in amphibole between pressures of 2 and 3.7 GPa and temperatures of
440 950 and 1100 °C can be expressed as a linear function of pressure and temperature (Figure 9):
441
442 $$(Na_2O + K_2O)_{amph} = -2.8616 + 1.0333\ P + 0.0037\ T \qquad R^2 = 0.98 \qquad (1)$$
443
444 where $(Na_2O + K_2O)_{amph}$ is the mol% abundance of $Na_2O + K_2O$ in amphibole on an anhydrous
445 basis, P is in GPa and T is in °C. The estimated error variance is 0.007. The mol% calculations
446 for amphibole do not include H_2O or halogens, allowing the conversion to be made directly from
447 electron microprobe data. The temperature sensitivity is relatively small, but the pressure effect
448 is large, so if temperature is known, pressure can be precisely predicted from amphibole
449 composition. This effectively tracks the up-pressure stabilization of the (K,Na)-richterite
450 component in pargasitic-edenitic amphiboles, and so holds potential as a geobarometer for
451 ultramafic rocks containing such amphiboles.
452 Figure 10 shows the predictive capability of this model for literature data on
453 experimentally produced amphiboles in peridotite bulk compositions. For relatively typical
454 fertile and depleted peridotites, this model provides very good fit even outside the calibration
455 range (< 2 GPa, < 950 °C); if the same regression is performed against all data, the fit is almost
456 identical, even outside the calibration range. Furthermore, the predictive capability of this model

457 is stronger than the scatter of the data suggests. This is because a similar amount of scatter is
458 observed even for individual studies that vary only pressure and temperature (e.g. Wallace and
459 Green 1991; Niida and Green 1999). These studies each scatter symmetrically around the model
460 prediction - so the model is accurately predicting the compositional variability - but the scatter is
461 not systematic with respect to pressure or temperature. This is unexpected, because if only
462 pressure and temperature are being varied then it is a thermodynamic requirement that amphibole
463 composition can only vary along two vectors in composition space (one each for pressure and
464 temperature), which is observed in our experiments and accounted for by our model. It is
465 therefore likely that much of the scatter observed in the literature data is due to experimental
466 irreproducibility or analytical uncertainty in those experiments, and that the model uncertainties
467 given in Figure 10 are maximum – and probably unrealistically high – errors. Whereas the mean
468 absolute error (MAE) for all of the experiments in Figure 10 is 0.24 GPa, the MAE for the
469 experiments from this study is only 0.06 GPa. The true uncertainty for high-quality microprobe
470 analyses of amphiboles is between these values.

471 The rest of the scatter can be ascribed to systematic differences between our experiments
472 and those plotted in Figure 10. These differences can help to constrain the range of conditions
473 over which our model may be applied to experimental and natural amphiboles. Three main
474 differences are observed:

475 1. H_2O. High abundances of free H_2O significantly decrease the stability field of
476 amphibole by leaching alkalis into a free fluid phase. It has been suggested that this leaching
477 decreases the alkali content of amphiboles at a given pressure and temperature (Green et al.
478 2014). However, this is not observed in our experiments (both the FNa and FNa3 experiments fit

our model equally well), and is not resolved by literature data for bulk H_2O contents lower than ~6 wt.% (Figure 10c). The main effect of alkali leaching appears to be on the stability of amphibole rather than its composition. However, for extremely high H_2O contents (the 14.5 wt.% H_2O experiments of Grove et al. (2006) and Green et al. (2014)), amphiboles are systematically depleted in alkalis relative to our model prediction (Figure 10c), indicating a small leaching effect on amphibole composition at very high bulk H_2O.

2. K_2O. This model is calibrated against experiments in which amphibole is the only major alkali-bearing mineral and the only significant site for potassium. In more K-rich systems, phlogopite is also stable, which sets up exchange reactions for alkalis (mostly K) between amphibole and phlogopite, with their own dependences on pressure and temperature. These are not accounted for by our model, so it is unsurprising that the phlogopite-bearing experiments of Mengel and Green (1989) and Fumagalli et al. (2009) are each systematically offset from our model predictions (Figure 10d: Mengel and Green = 0.43 wt.% K_2O; Fumagalli et al. = 0.54 wt.% K_2O). For phlogopite-free systems (all experiments below 0.1 wt.% bulk K_2O; Figure 10d), the bulk K_2O content has no effect, but the model is not calibrated for phlogopite-bearing peridotites. We therefore propose that this thermobarometer should be restricted to phlogopite-free assemblages or those with only accessory phlogopite.

3. CaO. The extremely Ca-poor composition of Pirard and Hermann (2015; bulk CaO = 0.29 wt.%) stabilizes a much more alkali-rich amphibole (Figure 10a). In most experiments on amphibole in peridotite, the M4 site is dominated by Ca because the bulk CaO/Na_2O ratio is high (> 4 in all compositions listed in Table 1 except that of Pirard and Hermann). However, in the experiments of Pirard and Hermann, this ratio is only 0.2, so the stable amphibole is Ca-poor,

(Na,K)-rich magnesiokatophorite. This indicates that our model is currently only applicable to pargasite-edenite-type amphiboles, which require a sufficiently high bulk CaO, or $CaO/(Na_2O+K_2O)$ ratio, to be stable. Our experiments on the depleted mantle composition DNa (CaO = 1.69 wt.%; $CaO/(Na_2O+K_2O)$ = 3.7) satisfy this requirement, as evidenced by their good fit to the model. Our model is therefore applicable to most amphibole-bearing depleted peridotites, with the possible exception of ultradepleted compositions.

Overall, this model is applicable to amphibole-bearing peridotites from 1 – 3.7 GPa and 800 – 1150 °C. It is calibrated for phlogopite-free systems with olivine, orthopyroxene and clinopyroxene, with or without an additional aluminous phase. Minor accessory phlogopite is unlikely to have an adverse effect, but if phlogopite is a major phase then its effect on the distribution of K may affect pressure estimates. The thermobarometer should also be applicable to clinopyroxene-free systems – our highest-temperature experiments are almost clinopyroxene-free – but sufficient Ca must be present to stabilize pargasite-edenite-type amphiboles over more Ca-poor, alkali-rich compositions.

Effects of H_2O on the stability and composition of amphibole

Many experiments conducted on peridotites have had much larger quantities of H_2O than is realistic for metasomatic processes likely to occur in much of the mantle. The water storage capacity of the solid mantle is high at low temperatures (>1 wt.%, and up to 2 wt.% in fully chloritized peridotite up to 840 °C; Grove et al. 2006; Till et al. 2012; Schmidt and Poli 2014), and at higher temperatures the presence of H_2O triggers the production of melts, which at mantle pressures have H_2O solubilities > 20 % (Hodges 1972; Pirard and Hermann 2015). The presence

523 of a significant free fluid phase during the production of amphibole in peridotites might be
524 important in the immediate vicinity of the slab-mantle interface but is unlikely for mantle
525 metasomatism further into the mantle wedge and in other parts of the Earth's mantle. This is an
526 important experimental consideration because the presence of free fluid destabilizes amphibole
527 by leaching alkalis from solid phases (Green et al. 2010, 2014).

528 One of the obstacles in quantifying the effects of free fluid on amphibole stability is that
529 many other variables have effects that remain unquantified. Different bulk compositions,
530 experimental procedures, analytical methods, and often uncontrolled or unmonitored oxygen
531 fugacities make it difficult to make significant quantitative statements beyond very broad
532 observations (e.g. Figure 1). However, the FNa and FNa3 studies presented here are identical
533 except for the abundance of H_2O, so they can be used to quantitatively determine the effects of
534 bulk H_2O content on amphibole stability.

535 Figure 11 shows the amphibole stability field from compositions FNa (0.65 wt.% H_2O),
536 FNa3 (3 wt.% H_2O), and the experiments of Grove et al. (2006; 14.5 wt.% H_2O). The Grove et
537 al. experiments and ours were both performed using identical experimental and analytical
538 procedures and so remove interlaboratory calibration issues. The Grove et al. experiments were
539 also performed on a fertile peridotite composition, but with lower alkali contents similar to those
540 in composition DNa (this study). It is possible that some of the decrease in amphibole stability in
541 these experiments relative to the FNa and FNa3 experiments is due to the lower alkali contents in
542 the Grove et al. bulk composition. The estimate provided here for the destabilizing effect of H_2O
543 at the highest H_2O contents (Figure 11b) should therefore be considered a maximum.

544 The effect of H_2O on the composition of amphibole is less clear. Green et al. (2010,
545 2014) noted that the presence of a fluid phase significantly decreases the Na_2O content of
546 clinopyroxene. A similar effect was proposed for amphibole, but the effect of up to 3 wt.% H_2O
547 is essentially unresolvable within analytical uncertainty (Figure 4 in Green et al. 2014). Indeed,
548 the amphiboles in our FNa3 experiments (3 wt.% H_2O) show no resolvable alkali depletion
549 relative to the FNa experiments (0.65 wt.% H_2O). However very high H_2O contents (>6 wt.%
550 H_2O) do produce resolvably alkali-depleted amphiboles (Figure 10c).
551 Our experiments show that amphibole compositions from experiments with a few percent
552 H_2O are similar to those with <1 wt.% H_2O, but the amphibole stability fields are not. Future
553 experiments aimed at exploring the stability and composition of not only amphibole but also
554 other alkali-bearing phases should ideally use bulk H_2O contents of less than 1 wt.%. An
555 exception would be for areas of extremely high fluid flux, such as the immediate supra-slab zone
556 and regions of deep fluid penetration in deeply faulted oceanic lithosphere. These strongly
557 hydrated regions are repeatedly fluxed by H_2O and so have locally low residual alkali contents
558 that will not stabilize amphibole to such high pressures and temperatures during subsequent
559 subduction.
560
561 *Applications to natural samples: uses and limitations*
562 To test our new thermobarometer on natural samples, we have applied it to the peridotites of the
563 Ulten Zone in the Upper Austroalpine of NE Italy, to which many existing thermobarometers
564 have been applied (Nimis and Morten 2000). Because most high-quality geobarometers are
565 based on garnet equilibria (e.g. Nimis and Grütter 2010), it is desirable to have

amphibole+garnet-bearing peridotites for this comparison. Equilibrium garnet and pargasitic to edenitic amphibole rarely occur together in peridotite samples. However, the peridotites of the Ulten Zone contain both phases, and are particularly amenable to the rigorous use of our thermobarometer because the amphibole is commonly present as a disseminated equilibrium phase (i.e. not just in veins). These rocks were spinel peridotites from the mantle wedge that became entrained by the subducting plate, metasomatized, and brought into the garnet stability field at relatively low temperatures (Nimis and Morten 2000). Pressure-temperature estimates typically range from 750-850 °C and 2.0-2.7 GPa (Rampone and Morten 2001). For the three amphibole-bearing peridotites analyzed by Nimis and Morten (2000) in their own thermobarometric analysis, our thermobarometer gives pressure estimates of 2.0-2.2 GPa at 850 °C, or 2.3-2.6 GPa at 750 °C. These estimates are in good agreement with those from existing thermobarometers and corroborate the utility and applicability of our new amphibole-based thermobarometer.

One of the potential uses for our new thermobarometer is the determination of equilibrium pressure conditions for metasomatized spinel peridotites, for which high-quality barometers remain elusive. The observation that the alkali-in-amphibole thermobarometer presented here reproduces experimental pressures down to 1 GPa (Figure 10b) suggests that this may be coupled with existing thermometers to provide reasonable pressure estimates for spinel peridotites.

We have calculated pressures for four studies of metasomatized spinel peridotites from various tectonic settings. We chose only examples of peridotites in which the amphibole is pargasitic and present as a disseminated phase. Amphiboles in or closely associated with veins

588 may provide erroneous pressure predictions because they are produced by an inherently
589 disequilibrium process: the diffusive reaction between a hydrous melt and a host rock of very
590 different composition. Conversely, peridotites with disseminated amphibole of consistent
591 composition typically represent complete reaction between a hydrous fluid and a host peridotite,
592 for which experiments provide a close proxy, and on which our thermobarometer may be used.
593 (1) St Paul's Rocks, equatorial Atlantic. This enormous oceanic core complex, which has
594 exposed mylonitized spinel peridotites above sea level, was studied in detail by Melson et al
595 (1972). Sample 18-900 from their study is a relatively fertile peridotite with mildly enriched
596 alkali contents and a spinel harzburgite lithology, and contains abundant pargasite and only
597 accessory phlogopite (bulk K_2O = 0.11 wt.%). Two-pyroxene thermometry from associated
598 peridotites (Roden et al. 1984) yields pressure-corrected temperature estimates of 960-1030 °C.
599 These temperatures combined with the amphibole composition from sample 18-900 yield a
600 pressure estimate of 1.5-1.7 GPa, consistent with estimates based on postulated geotherms from
601 Melson et al. (1972).
602 (2) Zabargad Island, Red Sea. Another peridotite-rich island exposed in an (incipient)
603 ocean, Zabargad hosts a wide range of mantle lithologies. Its fertile lherzolite units are
604 pervasively metasomatized and contain ubiquitous disseminated pargasite of quite consistent
605 composition (Agrinier et al. 1993). This metasomatic event is thought to predate the alteration
606 events associated with the exhumation of Zabargad. Based on the abundance of heavy Li
607 isotopes (Brooker et al. 2004), and Os-isotope melt extraction ages (Snow and Schmidt 1999),
608 the metasomatic event that produced these pargasites is thought to be related to subduction
609 processes during the Pan-African orogeny. Using an estimated equilibration temperature of 1000

610 °C from pyroxene thermometry (Piccardo et al. 1988), we calculate an equilibration pressure of
611 2.1 +- 0.1 GPa based on the composition of amphiboles from 6 peridotite samples.
612 (3) Victoria Land, Antarctica. Spinel lherzolite xenoliths from Baker Rocks contain
613 disseminated and vein pargasites that have recently been studied by Bonadiman et al. (2014).
614 These lherzolites are not very Na-enriched or deeply sourced (Na_{cpx} = 0.030-0.066 apfu),
615 allowing us to use the simple Brey and Köhler (1990) two-pyroxene thermometer, which
616 provides accurate temperature estimates for these general conditions (Nimis and Grütter 2010).
617 Focusing on the disseminated pargasite, we iterated temperatures obtained from the Brey and
618 Köhler thermometer – which requires a pressure term for its prediction – with pressure estimates
619 using our alkali-in-amphibole thermobarometer to obtain corrected temperature estimates of
620 990–1050 °C and pressure estimates of 2.2-2.6 GPa for six spinel lherzolites. Although this
621 pressure may appear too high for the spinel stability field, these lherzolites have very high bulk
622 Cr_2O_3/Al_2O_3 ratios, which increase the pressure of the spinel-garnet transition (O'Neill 1981;
623 Carroll Webb and Wood 1986; Klemme 2004; Ziberna et al. 2013). The Cr_2O_3/Al_2O_3 ratio of
624 composition FNa (this study, spinel-garnet transition between 2 and 2.5 GPa) is 0.10. The ratio
625 for composition DNa (this study, spinel-garnet transition greater than 2.5 GPa) is 0.23. The ratios
626 for the Bonadiman (2014) samples with the highest pressures predicted from our
627 thermobarometer are > 0.4, indicating a very high pressure (>>2.5 GPa) for the spinel-garnet
628 transition. Our pressure predictions are therefore consistent with these samples having last
629 equilibrated in the spinel stability field.
630 (4) Avacha volcano, Kamchatka arc. Mantle xenoliths reported from this volcano sample
631 the sub-arc mantle and are predominantly metasomatized harzburgites (Arai et al. 2003). A

precise temperature estimate for these harzburgites is not given by the authors, but is reported as 900 – 1000 °C as estimated from two-pyroxene thermometry. For a temperature of 900 °C, the composition of amphibole in the metasomatized harzburgite yields a pressure of 1.1 GPa, but for a temperature of 1000 °C, this estimate goes up to 1.5 GPa. This highlights the value of combining the alkali-in-amphibole thermobarometer with a precise geothermometer to achieve the most reliable pressure estimates.

Studies on all four of the localities discussed above have lamented the lack of an appropriate barometer for spinel peridotites. The pressures we have estimated here are consistent with all available information (spinel stability field, bulk composition, estimated geotherms), and as we improve our understanding of the factors controlling amphibole stability, these estimates will become increasingly precise. For the assemblage olivine + orthopyroxene + pargasitic amphibole ± clinopyroxene ± garnet/spinel, this thermobarometer already provides useful pressure estimates from 1 to 4 GPa. Of course, the mantle is a complex place, and the unusual compositional features observed in some mantle samples need to be incorporated into this model to extend its use to unusual compositions. Of particular interest moving forward are the effects of TiO_2, oxygen fugacity, halogens, bulk Na/K ratio, and amphibole-phlogopite equilibria.

Implications for water budgets in subduction zones and continental lithosphere

A comprehensive understanding of hydrous phase stability is necessary in the study of subduction zone and lithospheric dynamics, providing constraints on fluid transport and melt generation, the water storage capacity and water content of the upper mantle, and intraplate melting. In addition to providing a new tool for constraining the pressure-temperature conditions

of metasomatized peridotites, our experimental results also extend the amphibole stability field in fertile peridotite to ~0.5 GPa higher pressure than previous studies (Figure 12), and also indicate a large stability field for amphibole in truly depleted peridotites.

The mantle wedge immediately above the subducting slab is continuously fluxed by slab-derived fluids, and is therefore likely to be strongly alkali-leached. It is highly unlikely that amphibole is stable in this region to pressures above ~2 GPa (Grove et al. 2006). Parts of the mantle deep within the subducting slab itself may retain amphibole up to the stability limit in depleted peridotite (3-3.2 GPa).

Finally, it is worth noting that these new constraints provide updated inputs into models of water storage and release in thermally perturbed lithosphere. The stability of amphibole to higher pressure increases the overall water storage capacity of the lithosphere for a range of cratonic geotherms (Figs. 7 and 12). This may lead to deeper dehydration melting processes and thereby deeper generation of intraplate alkaline magmas.

Conclusions

1. The upper stability limit of pargasitic amphibole in fertile mantle peridotite has been redefined as 3.7–4.0 GPa, ~0.5 GPa higher (15 km deeper) than any previous studies. At ~1000 °C, this corresponds to conditions found in the sub-cratonic lithospheric mantle, indicating that pargasitic amphibole is stable to greater depths in the cratonic lithosphere. This indicates an expanded reservoir for water storage in the mantle, and extends the pressure range over which thermal perturbations may trigger melting due to water release associated with high-temperature amphibole breakdown.

2. Amphibole is stable to substantially lower pressure (3.0-3.2 GPa) in depleted peridotites. This supports previous studies that suggested that bulk composition affects amphibole stability, and will help models of hydrous phase stability to incorporate bulk composition.
3. The abundance of water in the peridotite system has a huge effect on the stability of amphibole, decreasing the upper pressure stability limit by ~0.2 GPa per wt.% H_2O. This has significant implications for the stability of amphibole at the interface between subducting slabs and the overlying mantle wedge, where high concentrations of water ascending through progressively depleted mantle may destabilize amphibole at very low pressures (<2 GPa). Strongly fluid-fluxed portions of the deep mantle wedge are therefore likely to be amphibole-free.
4. A new thermobarometer has been developed for amphibole-bearing peridotite. It is based on the alkali content of amphibole, and may be used at 1-4 GPa over a range of fertile and depleted peridotite compositions and bulk H_2O contents.

Acknowledgements

Thoughtful reviews from C. Pirard and P. Nimis, plus editorial handling from O. Müntener, led to improvements in this manuscript. This research was supported by National Science Foundation grants EAR-1118598 and EAR-1551321 to T.L. Grove.

References

Agrinier P, Mével C, Bosch D, Javoy M (1993) Metasomatic hydrous fluids in amphibole peridotites from Zabargad Island (Red Sea). Earth Planet Sci Lett 120:187-205.

Arai S, Ishimaru S, Okrugin VM (2003) Metasomatized harzburgite xenoliths from Avacha volcano as fragments of mantle wedge of the Kamchatka arc: Implication for the metasomatic agent. Island Arc 12:233-246.

Armstrong JT (1995) CITZAF – a package of correction programs for the quantitative electron microbeam X-ray analysis of thick polished materials, thin-films and particles. Microbeam Anal 4:177-200.

Ballhaus C, Berry RF, Green DH (1991) High pressure experimental calibration of the olivine-orthopyroxene-spinel oxygen geobarometer: implications for the oxidation state of the upper mantle. Contrib Mineral Petrol 107:27-40.

Bonadiman C, Nazzareni S, Coltorti M, Comodi P, Giuli G, Faccini B (2014) Crystal chemistry of amphiboles: implications for oxygen fugacity and water activity in lithospheric mantle beneath Victoria Land, Antarctica. Contrib Mineral Petrol 167:984.

Boyd FR, England JL (1960) Apparatus for phase equilibrium studies at pressure up to 50 kilobars and temperatures up to 1750 °C. J Geophys Res 65:741-748.

Brey GP, Köhler T (1990) Geothermobarometry in four-phase lherzolites II. New thermobarometers, and practical assessment of existing thermobarometers. J Petrol 31:1353-1378.

Brooker RA, James RH, Blundy JD (2004) Trace elements and Li isotope systematics in Zabargad peridotites: evidence of ancient subduction processes in the Red Sea mantle. Chem Geol 212:179-204.

Carroll Webb SA, Wood BJ (1986) Spinel-pyroxene-garnet relationships and their dependence on Cr/Al ratio. Contrib Mineral Petrol 92:471-480.

Ernst WG (1962) Synthesis, stability relations, and occurrence of riebeckite and riebeckite-arfvedsonite solid solutions. J Geol 70:689-736.

Foley S (1991) High-pressure stability of the fluor- and hydroxy-endmembers of pargasite and K-richterite. Geochim Cosmochim Acta 55:2689-2694.

Frost DJ, McCammon CA (2008) The redox state of Earth's mantle. Ann Rev Earth Planet Sci 36:389-420.

Fumagalli P, Poli S (2005) Experimentally determined phase relations in hydrous peridotites to 6.5 GPa and their consequences on the dynamics of subduction zones. J Petrol 46:555-578

Fumagalli P, Zanchetta S, Poli S (2009) Alkali in phlogopite and amphibole and their effects on phase relations in metasomatized peridotites: a high-pressure study. Contrib Mineral Petrol 158:723-737.

Gilbert MC (1966) Synthesis and stability relationships of ferropargasite. Am J Sci 264:698-742.

Gilbert MC (1969) Reconnaissance study of the stability of amphiboles at high pressure. Carnegie Inst Wash Year Book 67:167-170.

Green DH (1973) Experimental melting studies on a model upper mantle composition at high pressure under water-saturated and water-undersaturated conditions. Earth Planet Sci Lett 19:37-53.

Green DH, Hibberson WO, Kovács I, Rosenthal A (2010) Water and its influence on the lithosphere-asthenosphere boundary. Nature 467:448-452.

Green DH, Hibberson WO, Rosenthal A, Kovács I, Yaxley GM, Falloon TJ, Brink F (2014) Experimental study of the influence of water on melting and phase assemblages in the upper mantle. J Petrol 55:2067-2096.

753 Grove TL, Parman SW, Bowring SA, Price RC, Baker MB (2002) The role of an H_2O-rich fluid component in the
754 generation of primitive basaltic andesites and andesites from the Mt. Shasta region, N California. Contrib Mineral
755 Petrol 142:375-396.
756
757 Grove TL, Chatterjee N, Parman SW, Médard E (2006) The influence of H_2O on mantle wedge melting. Earth
758 Planet Sci Lett 19:37-53.
759
760 Hart SR, Zindler A (1986) In search of a bulk-Earth composition. Chem Geol 57(3-4):247-267.
761
762 Hodges FN (1972) Solubility of H_2O in forsterite melt at 20 kbar. Carnegie Inst Wash Year Book 72:495-497.
763
764 Johannes W, Bell PM, Mao HK, Boettcher AL, Chipman DW, Hays JF, Newton RS, Siefert F (1971) An
765 interlaboratory comparison of piston-cylinder pressure calibration using the albite-breakdown reaction. Contrib
766 Mineral Petrol 32:24-38.
767
768 Keppler H (1996) Constraints from partitioning experiments on the composition of subduction-zone fluids. Nature
769 380:237-240.
770
771 Klemme S (2004) The influence of Cr on the garnet-spinel transition in the Earth's mantle: experiments in the
772 system MgO-Cr_2O_3-SiO_2 and thermodynamic modelling. Lithos 77:639-646.
773
774 Konzett J, Ulmer P (1999) The stability of hydrous potassic phases in lherzolitic mantle – an experimental study to
775 9.5 GPa in simplified and natural bulk compositions. J Petrol 40:629-652.
776
777 Kress VC, Carmichael ISE (1991) The compressibility of silicate liquids containing Fe_2O_3 and the effect of
778 composition, temperature, oxygen fugacity and pressure on their redox states. Contrib Mineral Petrol 108:82-92.
779
780 Kushiro I (1970) Stability of amphibole and phlogopite in the upper mantle. Carnegie Inst Washington Year Book
781 68:245-247.
782
783 Lee C-TA, Luffi P, Chin EJ (2011) Building and destroying continental mantle. Annu Rev Earth Planet Sci 39:59-
784 90.
785
786 Longhi J (2005) Temporal stability and pressure calibration of barium carbonate and talc/pyrex pressure media in a
787 piston-cylinder apparatus. Am Mineral 90:206-218.
788
789 Medard E, McCammon CA, Barr JA, Grove TL (2008) Oxygen fugacity, temperature reproducibility, and H_2O
790 contents of nominally anhydrous piston-cylinder experiments using graphite capsules. Am Mineral 93:1838-1844.
791
792 Melson WG, Hart SR, Thompson G (1972) St. Paul's Rocks, Equatorial Atlantic: Petrogenesis, radiometric ages,
793 and implications on sea-floor spreading. Geol Soc Am Memoir 132:241-272.
794
795 Mengel K, Green DH (1989) Stability of amphibole and phlogopite in metasomatized peridotite under water-
796 saturated and water-undersaturated conditions. In: Kimberlites and related rocks. Geological Society of Australia
797 Special Publication 14:571-581.
798
799 Millhollen GL, Irving AJ, Wyllie PJ (1974) Melting interval of peridotite with 5.7 per cent water to 30 kilobars. J
800 Geol 82:575-587.
801
802 Mysen BO, Boettcher AL (1975) Melting of hydrous mantle: I. Phase relations of natural peridotite at high pressures
803 and temperatures with controlled activities of water, carbon dioxide and hydrogen. J Petrol 16:520-548.
804

Niida K, Green DH (1999) Stability and chemical composition of pargasitic amphibole in MORB pyrolite under upper mantle conditions. Contrib Mineral Petrol 135:18-40.

Nimis P, Morten L (2000) P-T evolution of 'crustal' garnet peridotites and included pyroxenites from Nonsberg area (upper Austroalpine), NE Italy: from the wedge to the slab. J Geodynamics 30:93-115.

Nimis P, Grütter H (2010) Internally consistent geothermometers for garnet peridotites and pyroxenites. Contrib Mineral Petrol 159:411-427.

O'Neill HStC (1981) The transition between spinel lherzolite and garnet lherzolite, and its use as a geobarometer. Contrib Mineral Petrol 77:185-194.

Piccardo GB, Messiga B, Vannucci R (1988) The Zabargad peridotite-pyroxenite association: petrological constraints on its evolution. Tectonophysics 150:135-162.

Pirard C, Hermann J (2015) Experimentally determined stability of alkali amphibole in metasomatised dunite at sub-arc pressures. Contrib Mineral Petrol 169:1.

Rampone E, Morten L (2001) Records of crustal metasomatism in the garnet peridotites of the Ulten Zone (Upper Austroalpine, Eastern Alps). J Petrol 42:207-219.

Roden MK, Hart SR, Frey FA, Melson WG (1984) Sr, Nd and Pb isotopic and REE geochemistry of St. Paul's Rocks: the metamorphic and metasomatic development of an alkali basalt mantle source. Contrib Mineral Petrol 85:376-390.

Scambelluri M, Philippot P (2001) Deep fluids in subduction zones. Lithos 55:213-227.

Schmidt MW, Poli S (2014) Devolatilization during subduction. In: Holland H, Turekian K, eds. Treatise on Geochemistry (2nd edition), 4:669-701.

Snow JE, Schmidt G (1999). Proterozoic melting in the northern peridotite massif, Zabargad Island: Os isotopic evidence. Terra Nova 11:45-50.

Stolper E, Newman S (1994) The role of water in the petrogenesis of Mariana trough magmas. Earth Planet Sci Lett, 121:293-325.

Syracuse EM, van Keken PE, Abers GA (2010) The global range of subduction zone thermal models. Phys Earth Planet Int 183:73-90.

Till CB, Grove TL, Withers AC (2012) The beginnings of hydrous mantle wedge melting. Contrib Mineral Petrol 163:669-688.

Tropper P, Manning CE, Essene EJ, Kao L-S (2000) The compositional variation of synthetic sodic amphiboles at high and ultra-high pressures. Contrib Mineral Petrol 139:146-162.

Tumiati S, Fumagalli P, Tinaboschi C, Poli S (2013) An experimental study on COH-bearing peridotite up to 3.2 GPa, and implications for crust-mantle recycling. J Petrol 54:453-479.

Van Keken PE, Hacker BR, Syracuse EM, Abers GA (2011) Subduction factory: 4. Depth-dependent flux of H_2O from subducting slabs worldwide. J Geophys Res 116:B01401.

Wada I, Behn MD, Shaw AM (2012) Effects of heterogeneous hydration in the incoming plate, slab rehydration, and mantle wedge hydration on slab-derived H_2O flux in subduction zones. Earth Planet Sci Lett, 353-354:60-71.

Walowski KJ, Wallace PJ, Hauri EH, Wada I, Clynne MA (2015) Slab melting beneath the Cascade Arc driven by dehydration of altered oceanic peridotite. Nat Geosci 8:404-408.

Wallace ME, Green DH (1991) The effect of bulk rock composition on the stability of amphibole in the upper mantle. Mineral Petrol 44:1-19.

Walter MJ (1999) Melting residues of fertile peridotite and the origin of cratonic lithosphere. In: Mantle petrology: Field observations and high pressure experimentation: A tribute to Francis R. (Joe) Boyd. Geochem Soc Spec Pub 6:225-239.

Yoder HS, Kushiro I (1969) Melting of a hydrous phase: phlogopite. Am J Sci 267A:558-582.

Ziberna L, Klemme S, Nimis P (2013) Garnet and spinel in fertile and depleted mantle: insights from thermodynamic modelling. Contrib Mineral Petrol 166:411-421.

Figure Captions

Fig. 1 Effect of H_2O on the upper pressure-temperature stability limit of pargasitic-edenitic amphibole in peridotite, from published experiments. Experiments with <5 wt.% H_2O stabilize amphibole to much higher pressures and temperatures than much wetter experiments. Stability fields from Kushiro (1970), Green (1973), Millhollen et al. (1974), Mysen and Boettcher (1975), Mengel and Green (1989), Wallace and Green (1991), Niida and Green (1999), Grove et al. (2006), Fumagalli et al. (2009), Tumiati et al. (2013)

Fig. 2 Compositions of starting materials used in this study (triangles) and prior studies (squares) compared to alkali-enriched (Na_2O > 0.4 wt.%, K_2O > 0.03 wt.%) peridotite samples from the GEOROC database (open circles). The grey field represents the depletion/re-enrichment trend populated by many peridotitic mantle xenoliths that are not alkali-enriched. See Table 1 for guide to symbols for experimental compositions

Fig. 3 Back-scattered electron images of run products. A and B: Run D274 (FNa, 1050 °C, 3 GPa), showing the typical appearance of the capsule section (A) and each phase (B). C: Run D296 (FNa, 1000 °C, 3.7 GPa), showing the presence of amphibole at 3.7 GPa. D: Run D293 (DNa, 1100 °C, 2 GPa), showing the appearance of spinel. Also shown in this panel is the typical appearance of quench amphibole, which grew from the melt phase during quenching of the experiment. Quench amphibole was identified in several 1100 °C experiments, based on its elongate habit, presence in voids, and melt-like chemistry (Mg# = 77)

Fig. 4 Phase diagrams for the three experimental series conducted in this study. All runs also contain olivine + orthopyroxene + clinopyroxene. See tables 1 and 2 for compositions of FNa, FNa3 and DNa. Curve indicates the upper pressure-temperature limit of amphibole stability. Grt-in represents the low-pressure stability limit of garnet. Size of symbols represents the estimated maximum experimental uncertainties (±10 °C, ±0.05 GPa)

Fig. 5 Compositions of experimental phases (in mol%) as a function of pressure at 1000 °C for the FNa bulk composition. Mg# = 100 * molar Mg/(Mg+Fe)

Fig. 6 Amphibole stability limit in fertile (FNa) vs. depleted (DNa) peridotite - this study

Fig. 7 Stability fields of amphiboles in a K-rich peridotite (0.54 wt.% K_2O, composition "B + Phl" in Table 1), from Konzett and Ulmer (1999; P = 6 - 9.5 GPa, T = 1100 - 1400 °C; squares) and Fumagalli et al. (2009; P = 1.5 - 5 GPa, T = 700 - 1000 °C; circles). Filled and open symbols

indicate the presence or absence of amphibole, respectively. High-temperature/low-pressure extension of Na-amphibole stability is estimated from existing studies cited in Table 1 (estimated uncertainty = ± 50 °C, 0.2 GPa). Red curve: hotter portions of the Nazca slab surface pressure-temperature profile from Syracuse et al. (2010; model D80). Sub-Cascadian and sub-Mexican slab surfaces also pass through the K-richterite stability field. Blue curve: 40 mW/m3 geotherm, representing the coldest geotherms through continental lithosphere (Lee et al., 2010)

Fig. 8 Schematic of controls on the upper pressure-temperature stability of amphibole in mantle peridotite. Not shown here are the effects of halogens, which are not addressed in this study and remain poorly constrained – fluorine in particular appears to stabilize amphiboles to higher temperatures and possibly pressures (Foley 1991), but much more work is required to fully constrain the effects of anions on amphibole stability. Th effect of fO_2 is small for relevant oxygen fugacities and amphibole compositions

Fig. 9 Correlation between pressure, temperature and molar $Na_2O + K_2O$ in amphiboles from this study. Plotted are all 19 amphibole-bearing experiments from FNa, FNa3 and DNa runs; no systematic deviation from this correlation is observed in any of the three series. Grid shows the planar fit defined by Equation (1). Grid increments are 0.1 GPa and 10 °C. Only 13 experiments are visible here; the other 6 plot just below the grid

Fig. 10 Predictive capabilities of the alkali-in-amphibole thermobarometer. (a) Predicted vs. measured molar $Na_2O + K_2O$ contents of experimental amphiboles synthesized in peridotite

compositions. Filled yellow circles: data from this study; filled black circles: literature data. (b) Predicted vs. measured pressures for the same amphiboles as (a). Grey ellipse highlights data from the extremely Ca-depleted bulk composition used by Pirard & Hermann (2015) - see text for details. (c) and (d) Difference between measured and modeled $Na_2O + K_2O$ contents of amphiboles as a function of bulk H_2O (c) or K_2O (d). The experiments with 14 wt.% bulk H_2O all have 0.03 wt.% bulk K_2O; the experiments with 0.43 wt.% bulk K_2O have 0.2-0.4 wt.% bulk H_2O; the experiments with 0.54 wt.% bulk K_2O have 1.5-5.0 wt.% bulk H_2O. Data from Mengel and Green (1989), Wallace and Green (1991), Niida and Green (1999), Grove et al. (2006), Fumagalli et al. (2009), Green et al. (2014), and new analyses from the Grove et al. (2006) experiments. Data from Pirard and Hermann (2015) are excluded from error estimates – see text

Fig. 11 Effect of bulk H_2O content on the upper pressure-temperature stability of amphibole in fertile peridotite. (a) Upper stability curves for experimental series FNa (0.65 wt.% H_2O) and FNa3 (3 wt.% H_2O), plus that of Grove et al. (2006; 14.5 wt.% H_2O), produced in the same lab for a fertile peridotite with slightly lower alkali contents and much higher H_2O. (b) Representation of data in (a) to show effect of H_2O on pressure- (solid black line) and temperature- (dashed blue line) stability. Error bars represent absolute uncertainty for pressure and maximum uncertainty for temperature. Curves should not be extrapolated to lower H_2O contents because no destabilizing effect has been resolved for H_2O contents significantly less than 1 wt.%

Fig. 12 Stability field of amphibole in fertile and depleted peridotite from this study (solid black lines) compared to previous experimental studies (dashed grey lines; references as in Figure 1). Grey region = range of cratonic geotherms determined from xenoliths, broadly corresponding to heat flows of 40-50 mW m^{-2} (Lee et al. 2011). Black region = range of slab surface temperatures for Mexico and the Cascades from the D80 model of Syracuse et al. (2010)

Table Captions

Table 1 Starting compositions (wt.%) used in mantle experiments that provide information on amphibole stability

Table 2 Experimental conditions and phase assemblages

Table 3 Amphibole compositions (wt.%) from experiments

Table 1 Starting compositions (wt.%) used in mantle experiments that provide information on amphibole stability

	This study		Other studies									
	FNa[1]	DNa[2]	MPY-40[3]	Tin-40[4]	HPY-40[5]	"C"[5]	M&B A[6]	M&B B	M&B C	M&B D	H&Z[7]	HZ2[8]
SiO_2	44.65	43.72	47.15	47.5	47.9	47.2	45.7	43.7	45.1	44.82	46.2	46.84
TiO_2	0.15	0.05	0.28	0.13	1.18	0.25	0.05	0.2	0.13	0.52	0.18	0.19
Al_2O_3	3.87	1.79	7.28	5.35	5.91	5.6	1.6	4	3.92	8.21	4.06	4.28
Cr_2O_3	0.37	0.42	0.75	0.75	0.72	1.08					0.4	0.42
FeO	8.14	7.97	7.27	7.52	8.81	6.69	5.9	8.89	8.19	9.77	7.56	4.14
MnO	0.14	0.13	0.12	0.18	0.13	0.07	0.09	0.12	0.14	0.19	0.1	0.1
MgO	37.70	42.82	30.57	32.8	28.8	33.59	42.8	37.4	38.81	26.53	37.82	39.8
CaO	3.38	1.69	5.63	4.97	5.14	4.43	0.7	3.5	2.66	8.12	3.22	3.39
Na_2O	0.62	0.40	0.66	0.3	0.95	0.35	0.09	0.38	0.27	0.89	0.33	0.35

K_2O	0.08	0.06	0	0.03	0.22	0.43	0.04	0.01	0.02	0.03	0.03	0.03
NiO	0.25	0.30	0.29	0.43	0.13	0.3	0.26	0.24	0.25	0.2	0.28	0.29
H_2O added	0.65 & 3	0.65	0.6-0.7	0.2 & 1	0.3 & 10	0.15-0.4	11-25	8-38	14-38	13-36	0-14.5[7]	0-14.5
Natural / Synthetic	Syn	Syn	Syn	Syn	Syn	Syn	Nat	Nat	Nat	Nat	Syn	Syn
Symbol in Figure 2	Open triangle	Filled triangle	Yellow square	Dark blue square	Black square	Grey square	Green triangle	Green triangle	Green triangle		Open square	

[1]Representative fertile mantle composition from the GEOROC database of mantle xenoliths, plus 1 wt.% of a metasomatic fluid composed of 65 wt.% H_2O, 30 wt.% N

[2]Representative depleted mantle determined from the GEOROC database of mantle xenoliths, plus 1 wt.% of a metasomatic fluid composed of 65 wt.% H_2O, 30 wt.%

[3]MORB pyrolite minus 40 % olivine, from Niida and Green (1999)

[4]Tinaquillo lherzolite minus 40 % olivine, from Wallace and Green (1991)

[5]Composition C from Mengel and Green (1989): average depleted spinel peridotite from the North Hessian Depression, NW Germany, plus 1.5 % phlogopite, minus 6

[6]Compositions M&B A, B, C and D are natural lherzolites from Mysen and Boettcher (1975).

[7]Estimated primitive mantle from Hart and Zindler (1986). Used in Grove et al. (2006; 14.5 wt.% H_2O), Green et al. (2010, 2014; 0-1.45 wt.% H_2O), and Till et al. (201

[8]Hart & Zindler (1986) primitive mantle composition, but with significant Fe depletion. From Green et al. (2010; 2014)

[9]Mildly depleted lherzolite -30 % olivine +5 wt.% phlogopite +0.4 wt.% Na_2O. From Konzett and Ulmer (1999); used in KNCFMASH by Fumagalli et al. (2009) and T

[10]Pargasite-rich spinel peridotite mylonite from St. Paul's Rocks containing 5.7 wt.% H_2O bound in hydrous minerals. From Millhollen et al. (1974).

[11]Mixture of 75% San Carlos olivine + 25% sediment melt. From Pirard and Hermann (2015).

969

970

Table 2 Experimental conditions and phase assemblages

Run	Starting Material	Duration (hr)	T (°C)	P (GPa)	Bulk H_2O (wt%)	Anhydrous phases	Hydrous phases
D278	FNa	167	950	3	0.65	Ol, opx, cpx, grt	amph
D263	FNa	165	1000	2	0.65	Ol, opx, cpx	amph
D264	FNa	163	1000	2.5	0.65	Ol, opx, cpx, grt	amph
D267	FNa	168	1000	3	0.65	Ol, opx, cpx, grt	amph
D281	FNa	165	1000	3.5	0.65	Ol, opx, cpx, grt	amph
D296	FNa	163	1000	3.7	0.65	Ol, opx, cpx, grt	amph
D310	FNa	147	1000	4	0.65	Ol, opx, cpx, grt	-
D265	FNa	167	1050	2	0.65	Ol, opx, cpx	amph
D272	FNa	168	1050	2.5	0.65	Ol, opx, cpx, grt	amph
D274	FNa	168	1050	3	0.65	Ol, opx, cpx, grt	amph
D285	FNa	142	1050	3.5	0.65	Ol, opx, cpx, grt	amph

D289	FNa	169	1050	3.7	0.65	Ol, opx, cpx, grt	-
D282	FNa	142	1100	2	0.65	Ol, opx, cpx	amph
D280	FNa	162	1100	2.5	0.65	Ol, opx, cpx, grt	amph
D286	FNa	95	1100	3	0.65	Ol, opx, cpx, grt	-
D283	FNa	120	1100	3.5	0.65	Ol, opx, cpx, grt	-
D298	FNa3[1]	170	1000	3	3	Ol, opx, cpx, grt	amph
D305	FNa3	141	1000	3.2	3	Ol, opx, cpx, grt	amph
D308	FNa3	167	1000	3.5	3	Ol, opx, cpx, grt	-
D299	FNa3	139	1050	2	3	Ol, opx, cpx	amph
D302	FNa3	148	1050	2.5	3	Ol, opx, cpx, grt	amph
D309	FNa3	144	1050	3	3	Ol, opx, cpx, grt	-
D311	FNa3	146	1075	2.5	3	Ol, opx, cpx, grt	-
D304	FNa3	142	1100	2	3	Ol, opx, cpx, sp	-
D295	DNa	120	1000	2	0.65	Ol, opx, cpx	amph
D297	DNa	170	1000	3.2	0.65	Ol, opx, cpx, grt	-
D291	DNa	163	1000	3.5	0.65	Ol, opx, cpx, grt	-
D288	DNa	167	1050	2.5	0.65	Ol, opx, cpx, sp	amph
D290	DNa	166	1050	3	0.65	Ol, opx, cpx, grt	amph
D293	DNa	140	1100	2	0.65	Ol, opx, cpx, sp	-
D292	DNa	168	1100	2.5	0.65	Ol, opx, cpx, sp	-

ol = olivine; *opx* = orthopyroxene; *cpx* = clinopyroxene; *grt* = garnet; *sp* = spinel; *amph* = amphibole

All runs also contain a melt phase

[1]FNa3 consists of composition FNa with additional H_2O added to give 3 wt.% H_2O in the bulk

971

972

Table 3 Amphibole compositions (wt.%) from experiments

Run No.	Bulk	T (°C)	P (GPa)	n[1]	**SiO_2**	SiO_2 1σ[2]	**TiO_2**	TiO_2 1σ	**Al_2O_3**	Al_2O_3 1σ	**Cr_2O_3**	Cr_2O_3 1σ	**FeO**	FeO 1σ	**MnO**	MnO 1σ	**MgO**	MgO 1σ	**CaO**	C
D278	FNa	950	3	9	**46.5**	0.9	**0.54**	0.05	**12.0**	0.7	**1.41**	0.12	**3.67**	0.09	**0.08**	0.02	**19.8**	0.6	**10.5**	
D263	FNa	1000	2	12	**45.4**	0.5	**0.54**	0.04	**14.1**	0.2	**1.18**	0.12	**3.69**	0.10	**0.08**	0.03	**18.6**	0.2	**11.4**	
D264	FNa	1000	2.5	12	**45.6**	0.3	**0.57**	0.04	**13.9**	0.4	**1.28**	0.13	**3.71**	0.08	**0.08**	0.01	**18.6**	0.2	**11.3**	
D267	FNa	1000	3	13	**46.9**	0.4	**0.61**	0.05	**12.0**	0.3	**1.19**	0.21	**3.44**	0.09	**0.07**	0.01	**19.5**	0.3	**10.4**	
D281	FNa	1000	3.5	17	**49.2**	0.4	**0.68**	0.05	**10.5**	0.2	**1.11**	0.10	**3.24**	0.10	**0.06**	0.02	**19.8**	0.4	**9.10**	

D296	FNa	1000	3.7	12	**48.3**	0.9	**0.66**	0.08	**10.0**	0.7	**1.07**	0.17	**3.41**	0.10	**0.07**	0.02	**21.2**	0.5	**8.8**	0
D265	FNa	1050	2	11	**45.9**	0.3	**0.54**	0.03	**14.0**	0.2	**1.20**	0.13	**3.72**	0.13	**0.08**	0.01	**18.6**	0.2	**11.4**	0
D272	FNa	1050	2.5	15	**45.9**	0.5	**0.62**	0.03	**13.7**	0.4	**1.22**	0.18	**3.72**	0.07	**0.09**	0.02	**18.7**	0.4	**11.0**	0
D274	FNa	1050	3	14	**46.9**	0.7	**0.74**	0.06	**11.8**	0.3	**1.31**	0.12	**3.61**	0.08	**0.08**	0.02	**19.0**	0.4	**10.1**	0
D285	FNa	1050	3.5	8	**47.3**	0.5	**0.72**	0.06	**10.4**	0.1	**0.95**	0.07	**3.54**	0.07	**0.06**	0.02	**20.7**	0.3	**8.7**	0
D282	FNa	1100	2	17	**44.0**	0.6	**0.64**	0.04	**14.3**	0.3	**1.67**	0.15	**3.48**	0.06	**0.09**	0.01	**19.6**	0.5	**10.7**	0
D280	FNa	1100	2.5	14	**44.0**	0.6	**0.59**	0.03	**14.4**	0.3	**1.29**	0.12	**3.64**	0.08	**0.08**	0.01	**19.7**	0.5	**10.3**	0
D298	FNa3	1000	3	12	**45.6**	0.6	**0.75**	0.10	**11.8**	0.3	**1.25**	0.19	**3.55**	0.05	**0.06**	0.01	**20.2**	0.4	**10.2**	0
D305	FNa3	1000	3.2	11	**46.2**	0.6	**0.74**	0.11	**11.6**	0.5	**1.25**	0.14	**3.61**	0.08	**0.07**	0.02	**20.3**	0.5	**9.8**	0
D299	FNa3	1050	2	18	**44.2**	0.7	**0.59**	0.03	**14.3**	0.2	**1.45**	0.16	**3.71**	0.07	**0.07**	0.01	**19.5**	0.4	**11.1**	0
D302	FNa3	1050	2.5	16	**44.2**	0.6	**0.61**	0.06	**14.1**	0.5	**1.35**	0.20	**3.64**	0.06	**0.06**	0.01	**19.4**	0.3	**10.7**	0
D295	DNa	1000	2	11	**46.2**	0.5	**0.40**	0.02	**11.6**	0.3	**2.14**	0.26	**3.21**	0.13	**0.08**	0.01	**21.1**	0.8	**10.7**	0
D288	DNa	1050	2.5	13	**45.0**	0.4	**0.40**	0.03	**12.7**	0.1	**1.85**	0.19	**3.83**	0.12	**0.08**	0.02	**19.7**	0.2	**10.4**	0
D290	DNa	1050	3	19	**45.2**	0.6	**0.49**	0.05	**12.6**	0.4	**1.86**	0.25	**4.15**	0.21	**0.07**	0.01	**19.6**	0.4	**10.0**	0

[1]Number of analyses

[2]One standard deviation of the analyses for this oxide

[3]Mg# = 100 * molar Mg/(Mg+Fe)

973

974

975

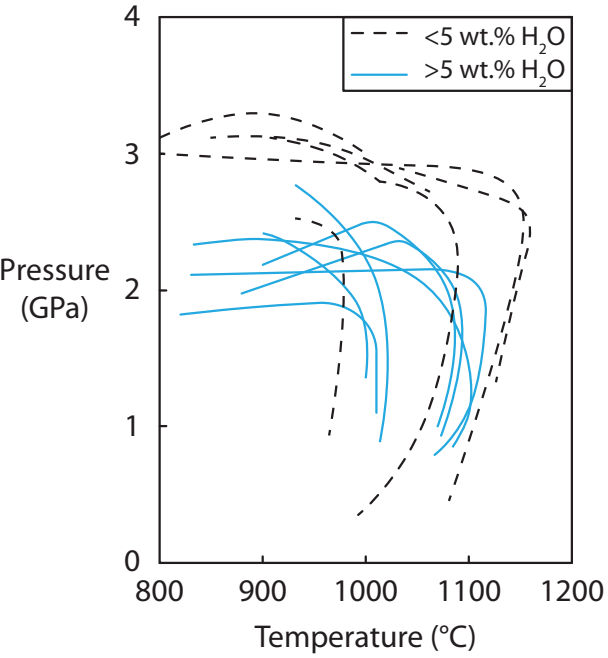
<5 wt.% H2O
>5 wt.% H2O
Pressure (GPa)
0
1
2
3
4
800
900
1000
1100
1200
Temperature (°C)

Figure 1

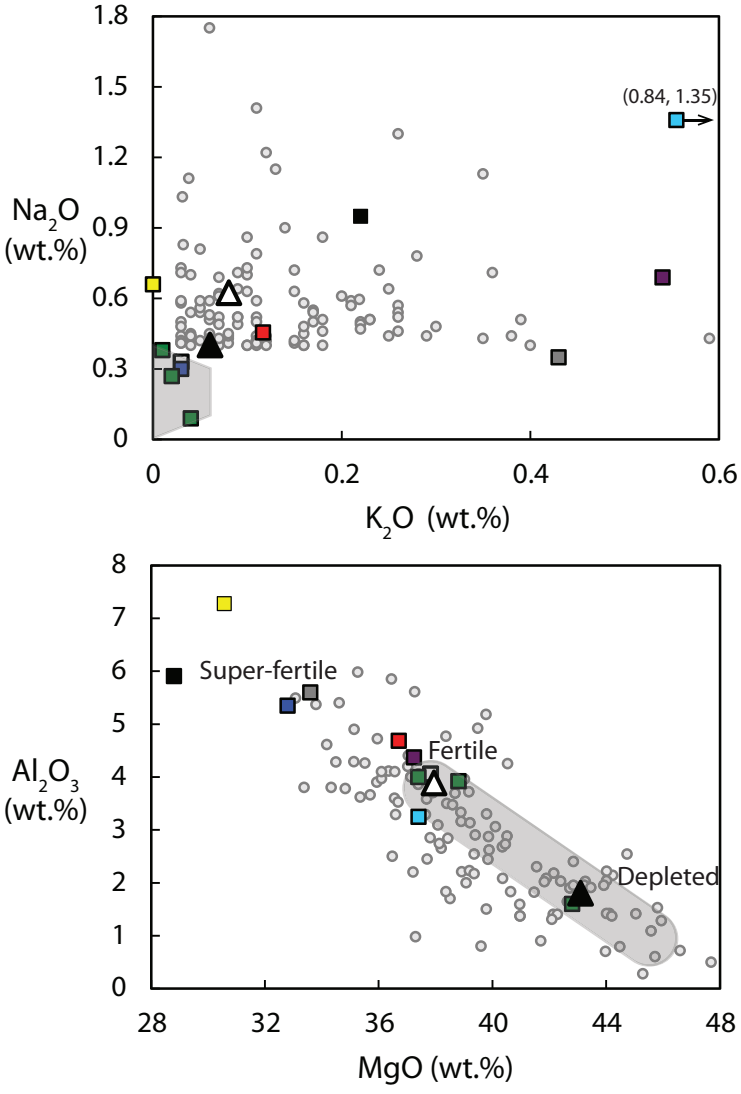
1.8
1.5
1.2
0.9
0.6
0.3
0
Na2O (wt.%)
(0.84, 1.35)
0
0.2
0.4
0.6
K2O (wt.%)
8
7
6
5
4
3
2
1
0
Al2O3 (wt.%)
Super-fertile
Fertile
Depleted
28
32
36
40
44
48
MgO (wt.%)

Figure 2

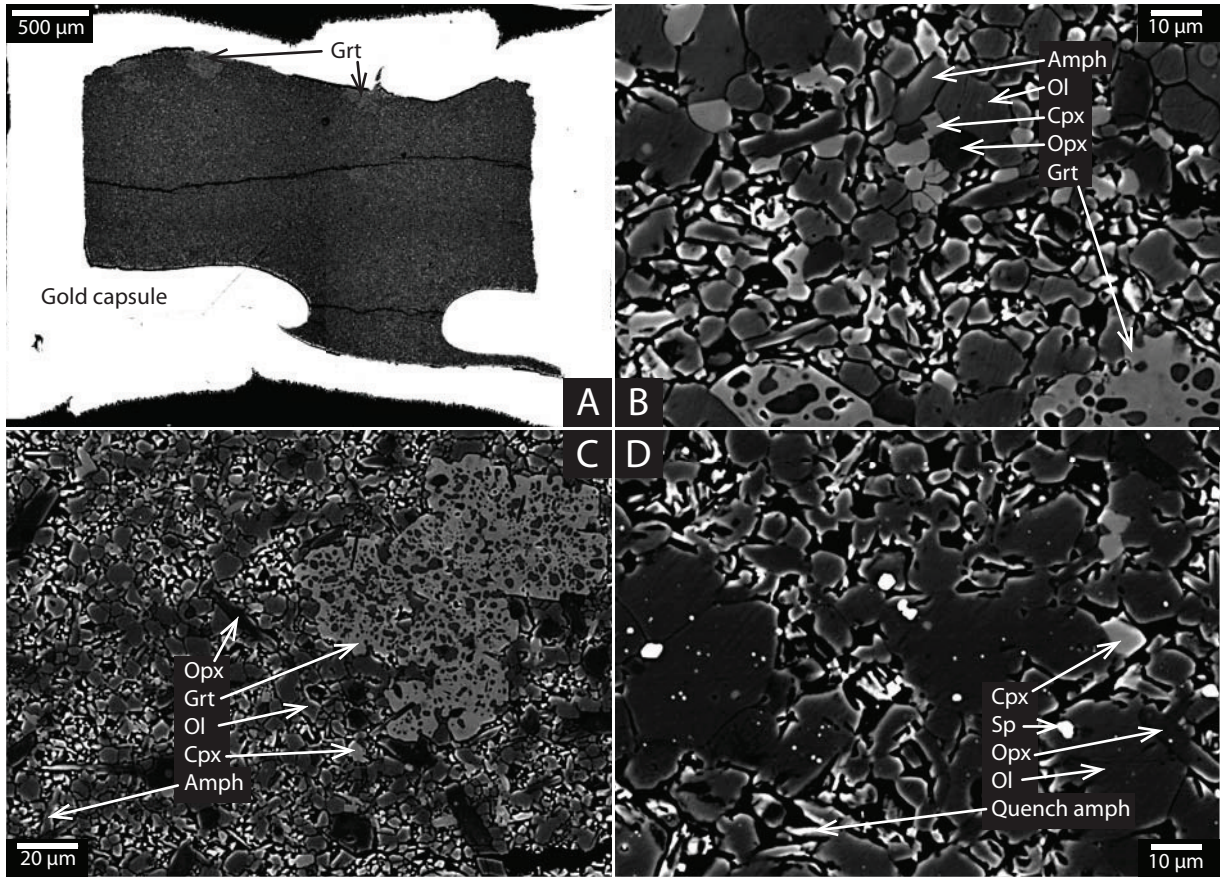
500 µm
Grt
Gold capsule
A
10 µm
Amph
Ol
Cpx
Opx
Grt
B
C
Opx
Grt
Ol
Cpx
Amph
20 µm
D
Cpx
Sp
Opx
Ol
Quench amph
10 µm

Figure 3

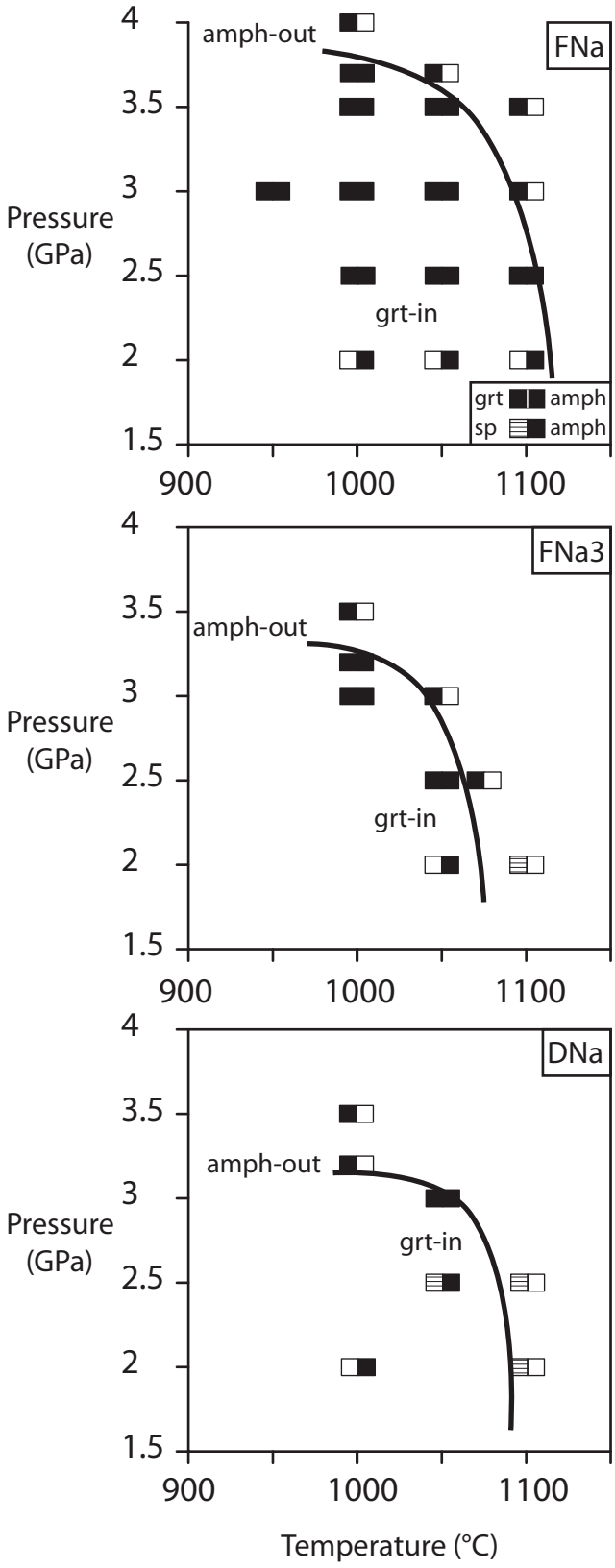
FNa
amph-out
grt-in
grt amph
sp amph
FNa3
amph-out
grt-in
DNa
amph-out
grt-in
Pressure (GPa)
Temperature (°C)
4
3.5
3
2.5
2
1.5
900
1000
1100

Figure 4

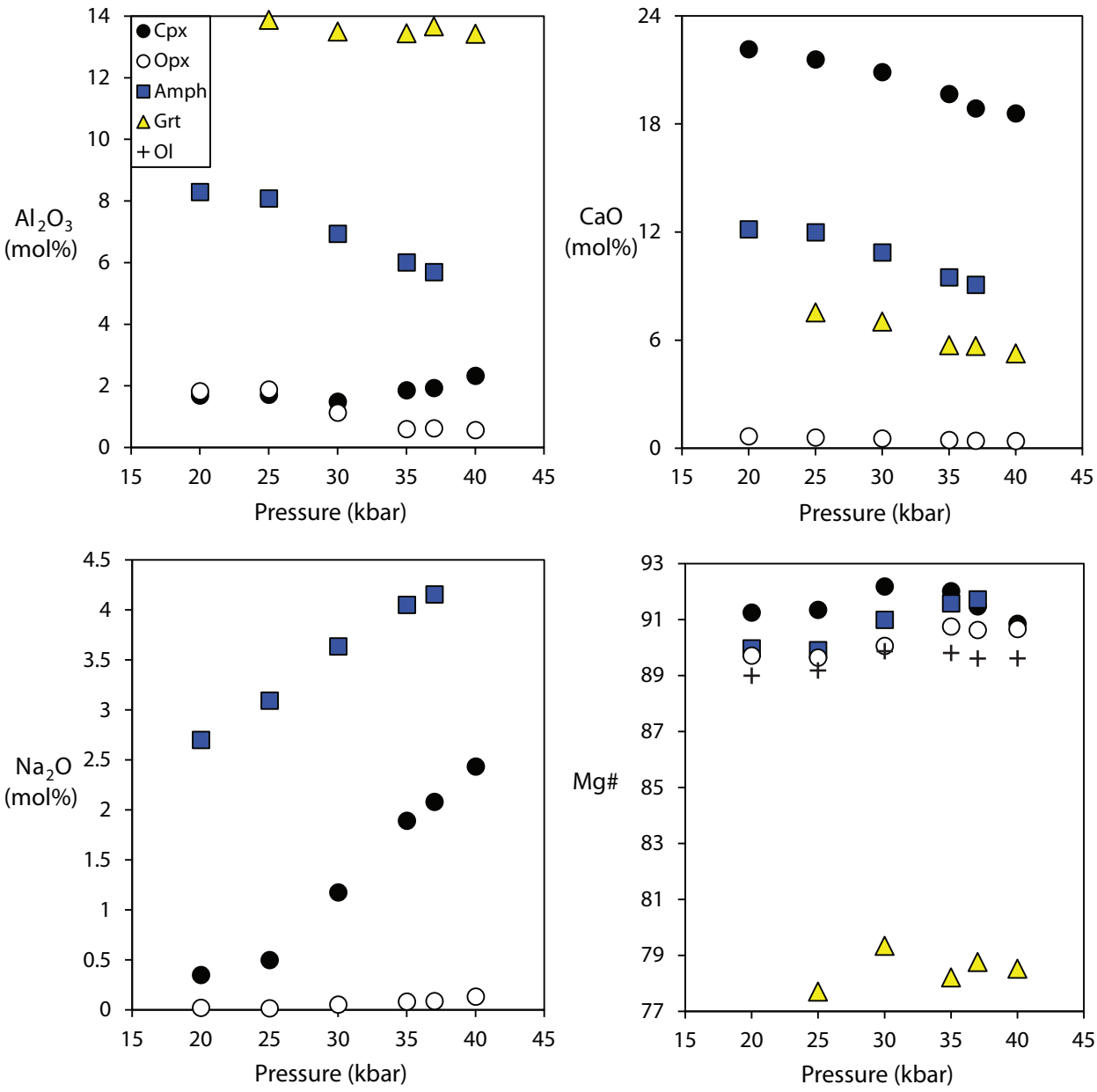
Cpx
Opx
Amph
Grt
Ol
Al2O3 (mol%)
CaO (mol%)
Na2O (mol%)
Mg#
Pressure (kbar)

Figure 5

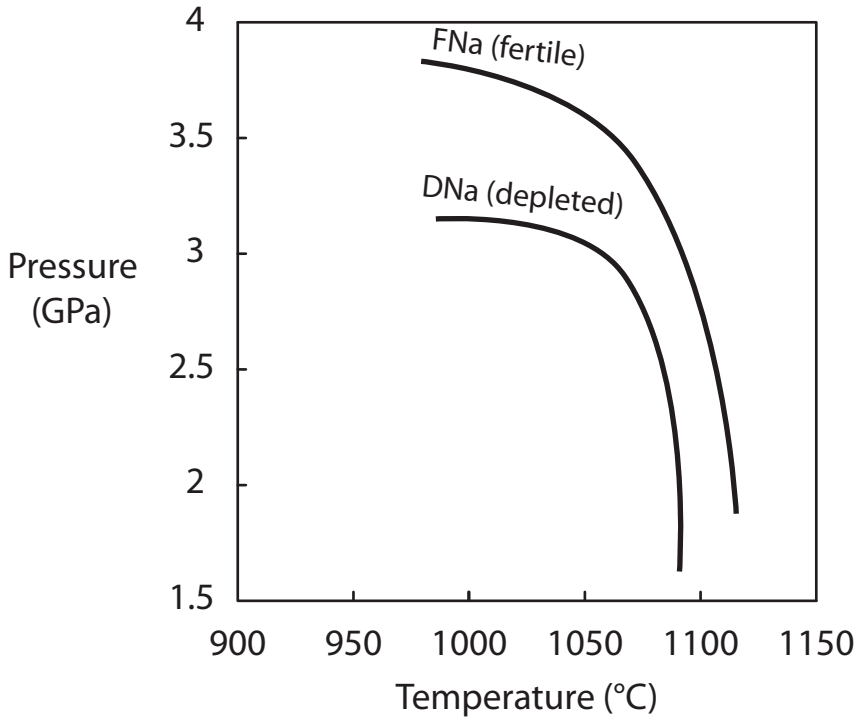
4
3.5
3
2.5
2
1.5
Pressure
(GPa)
FNa (fertile)
DNa (depleted)
900
950
1000
1050
1100
1150
Temperature (°C)

Figure 6

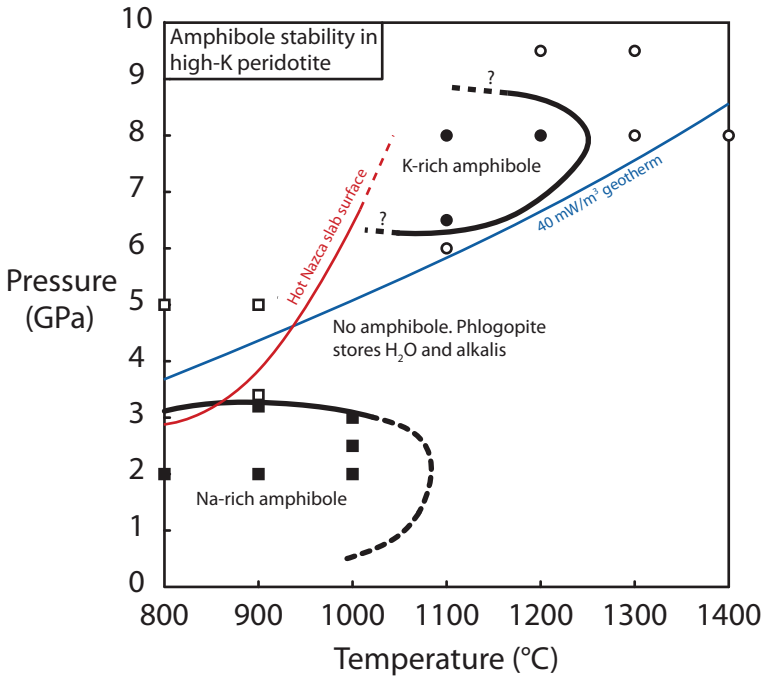
Amphibole stability in high-K peridotite
K-rich amphibole
Hot Nazca slab surface
40 mW/m² geotherm
No amphibole. Phlogopite stores H2O and alkalis
Na-rich amphibole
Pressure (GPa)
Temperature (°C)
0
1
2
3
4
5
6
7
8
9
10
800
900
1000
1100
1200
1300
1400

Figure 7

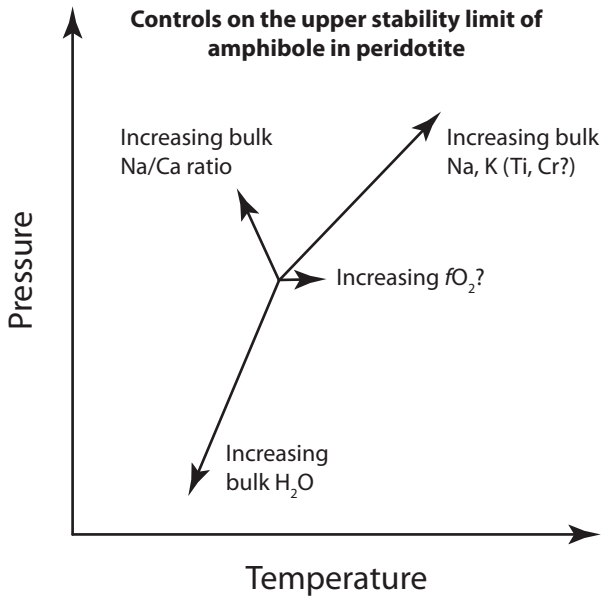
Controls on the upper stability limit of amphibole in peridotite
Increasing bulk Na/Ca ratio
Increasing bulk Na, K (Ti, Cr?)
Increasing fO_2?
Increasing bulk H_2O
Pressure
Temperature

Figure 8

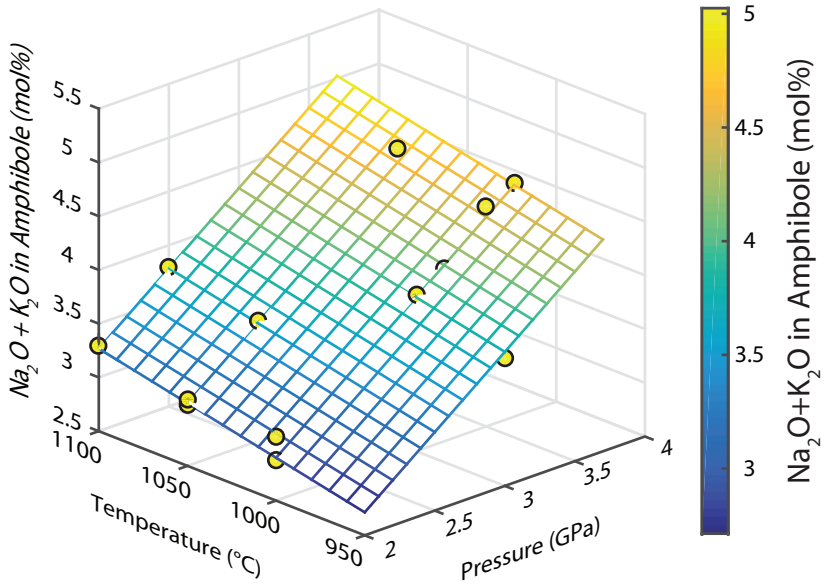
$Na_2O + K_2O$ in Amphibole (mol%)
5.5
5
4.5
4
3.5
3
2.5
1100
1050
1000
950
Temperature (°C)
2
2.5
3
3.5
4
Pressure (GPa)
5
4.5
4
3.5
3
Na_2O+K_2O in Amphibole (mol%)

Figure 9

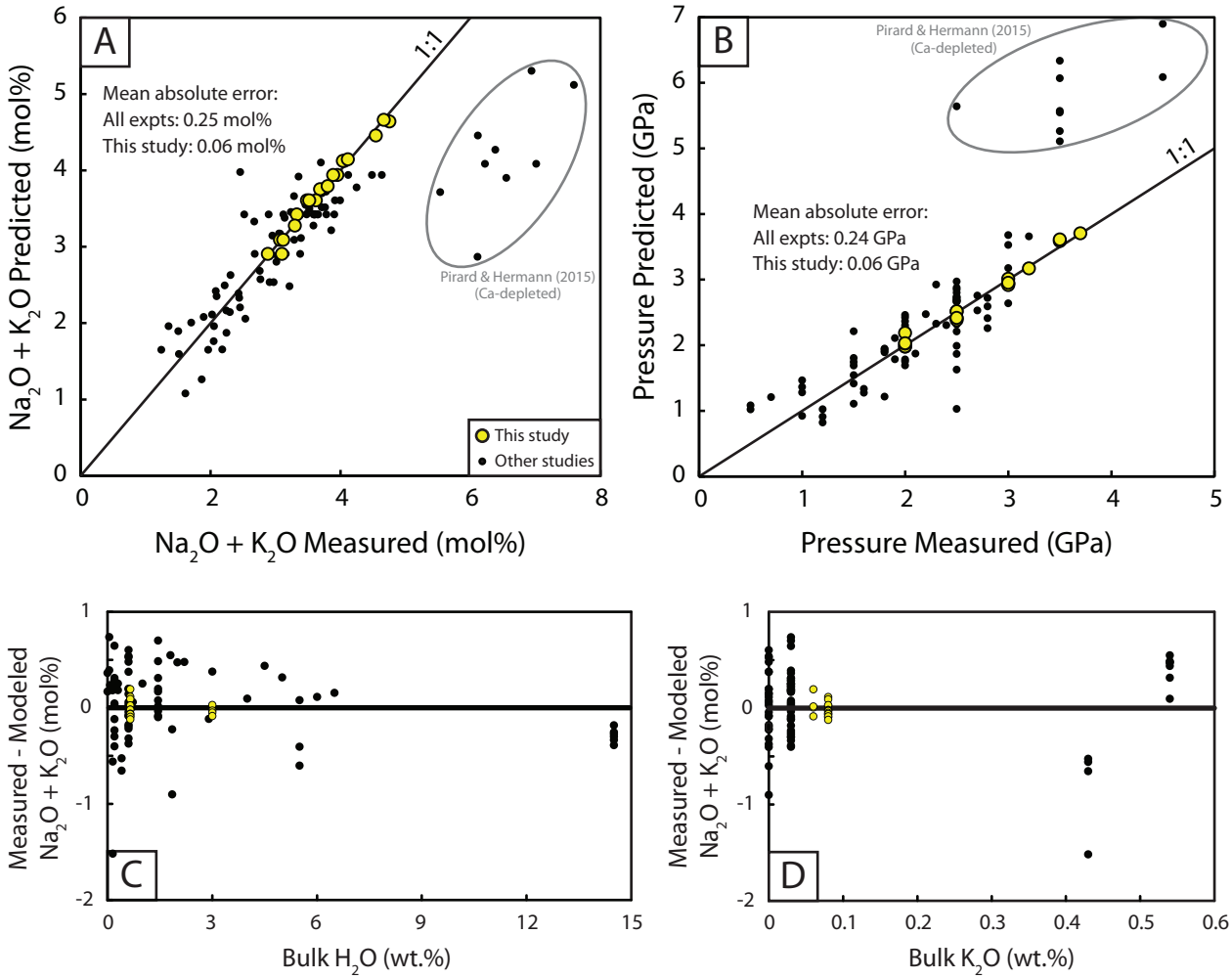
A
Mean absolute error:
All expts: 0.25 mol%
This study: 0.06 mol%
1:1
Pirard & Hermann (2015)
(Ca-depleted)
This study
Other studies
Na2O + K2O Predicted (mol%)
Na2O + K2O Measured (mol%)
B
Pirard & Hermann (2015)
(Ca-depleted)
Mean absolute error:
All expts: 0.24 GPa
This study: 0.06 GPa
1:1
Pressure Predicted (GPa)
Pressure Measured (GPa)
C
Measured - Modeled
Na2O + K2O (mol%)
Bulk H2O (wt.%)
D
Measured - Modeled
Na2O + K2O (mol%)
Bulk K2O (wt.%)

Figure 10

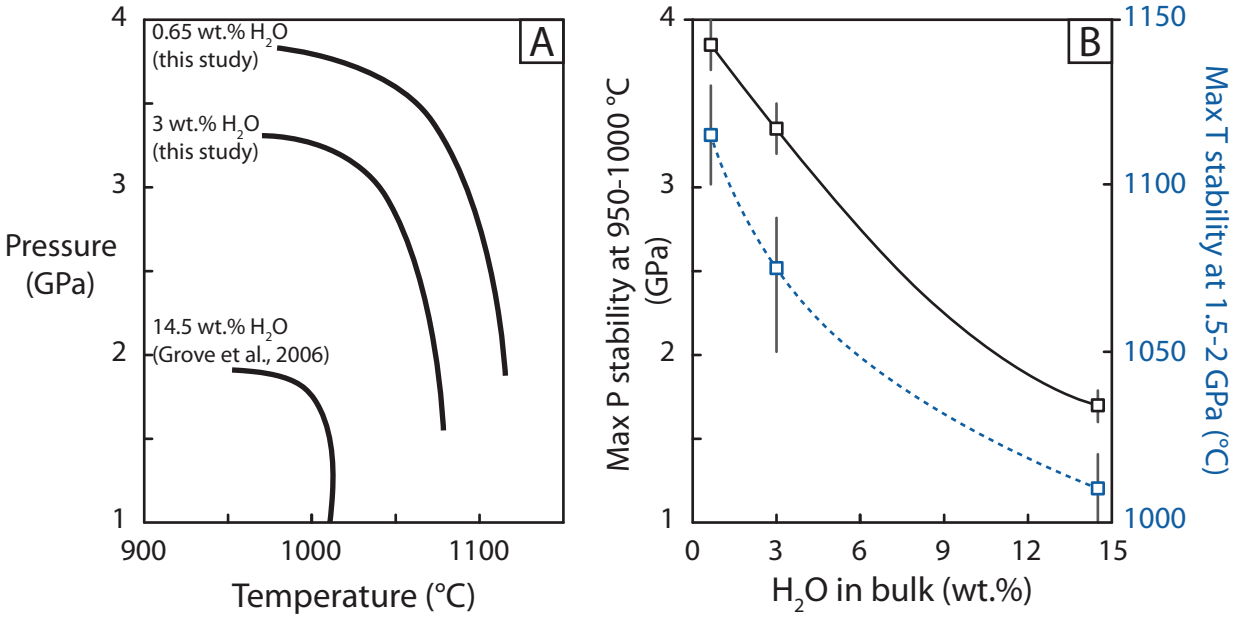
A
0.65 wt.% H2O
(this study)
3 wt.% H2O
(this study)
14.5 wt.% H2O
(Grove et al., 2006)
Pressure
(GPa)
Temperature (°C)
B
Max P stability at 950-1000 °C
(GPa)
Max T stability at 1.5-2 GPa (°C)
H2O in bulk (wt.%)

Figure 11

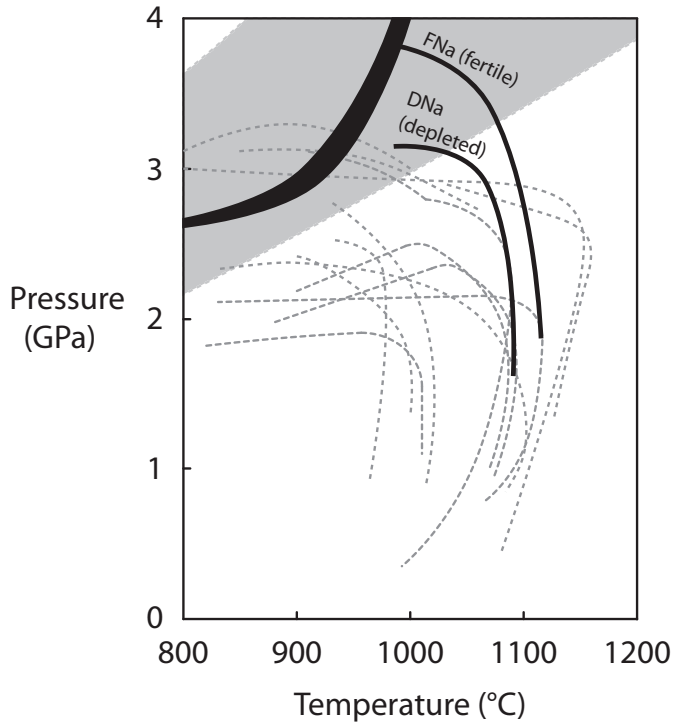
FNa (fertile)
DNa
(depleted)
Pressure
(GPa)
4
3
2
1
0
800
900
1000
1100
1200
Temperature (°C)

Figure 12